Cellular/Molecular

Use-Dependent, Untapped Dual Kinase Signaling Localized in Brain Learning Circuitry

James C. Sears[1,2] and Kendal Broadie[1,2,3,4]
[1]Vanderbilt Brain Institute, Departments of [2]Biological Sciences, [3]Cell and Developmental Biology and [4]Vanderbilt Kennedy Center, Vanderbilt University and Medical Center, Nashville, Tennessee 37235

Imaging brain learning and memory circuit kinase signaling is a monumental challenge. The separation of phases-based activity reporter of kinase (SPARK) biosensors allow circuit-localized studies of multiple interactive kinases in vivo, including protein kinase A (PKA) and extracellular signal-regulated kinase (ERK) signaling. In the precisely-mapped *Drosophila* brain learning/memory circuit, we find PKA and ERK signaling differentially enriched in distinct Kenyon cell connectivity nodes. We discover that potentiating normal circuit activity induces circuit-localized PKA and ERK signaling, expanding kinase function within new presynaptic and postsynaptic domains. Activity-induced PKA signaling shows extensive overlap with previously selective ERK signaling nodes, while activity-induced ERK signaling arises in new connectivity nodes. We find targeted synaptic transmission blockade in Kenyon cells elevates circuit-localized ERK induction in Kenyon cells with normally high baseline ERK signaling, suggesting lateral and feedback inhibition. We discover overexpression of the pathway-linking Meng-Po (human SBK1) serine/threonine kinase to improve learning acquisition and memory consolidation results in dramatically heightened PKA and ERK signaling in separable Kenyon cell circuit connectivity nodes, revealing both synchronized and untapped signaling potential. Finally, we find that a mechanically-induced epileptic seizure model (*easily shocked* "bang-sensitive" mutants) has strongly elevated, circuit-localized PKA and ERK signaling. Both sexes were used in all experiments, except for the hemizygous male-only seizure model. Hyperexcitable, learning-enhanced, and epileptic seizure models have comparably elevated interactive kinase signaling, suggesting a common basis of use-dependent induction. We conclude that PKA and ERK signaling modulation is locally coordinated in use-dependent spatial circuit dynamics underlying seizure susceptibility linked to learning/memory potential.

Key words: **circuit plasticity; epilepsy; ERK; learning; PKA; SBK1**

Significance Statement

Critical protein kinases act in learning/memory circuits to enable experience-dependent plasticity. This work images kinase signaling in vivo to elucidate circuit-level organization relative to mapped connectivity nodes. We discover different kinases exhibit heightened signaling in different circuit domains, which is dramatically reorganized by use-dependent synaptic transmission and circuit activity levels. We discover the newest learning/memory kinase, Meng-Po/SBK1, co-regulates different kinases within distinct circuit connectivity nodes. Targeted over-expression of Meng-Po/SBK1 improves learning and memory, and elevates kinase signaling, indicating untapped kinase signaling potential may enhance capabilities to learn and remember. Linked heightened seizure susceptibility similarly increases kinase signaling in learning/memory circuitry, indicating a trade-off of benefit for instability. This work mechanistically connects hyperexcitation seizure susceptibility and learning/memory via circuit-level kinase signaling.

Received June 16, 2023; revised Jan. 12, 2024; accepted Jan. 16, 2024.

Author contributions: J.C.S. and K.B. designed research; J.C.S. performed research; J.C.S. analyzed data; J.C.S. and K.B. wrote the paper.

We are very grateful to Xiaokun Shu (University of California, San Francisco, CA, USA) for UAS-SPARK lines, Brian McCabe (Brain Mind Institute, EPFL, Lausanne, Switzerland) for UAS-TNT lines, and Barry Ganetzky (University of Wisconsin, Madison, WI, USA) for the *eas*^{2} mutant. We are grateful to the Bloomington *Drosophila* Stock Center for providing essential lines and the Developmental Studies Hybridoma Bank for essential antibodies. We thank Neel Gundavarapu for technical contributions using Trio antibody labeling, and to other Broadie lab members for helpful input. This work was supported by NIH grants MH084989 and NS131557 (to K.B.), and Vanderbilt Brain Institute Trans-Institutional Program (TIPs) funding (to J.C.S. and K.B.).

The authors declare no competing financial interests.

Correspondence should be addressed to Kendal Broadie at kendal.broadie@vanderbilt.edu.

https://doi.org/10.1523/JNEUROSCI.1126-23.2024

Introduction

Brain circuits use interactive kinase signaling to regulate the synaptic connectivity plasticity enabling behavioral adaptations like learning and memory (Giese and Mizuno, 2013; Lee, 2015; Khan et al., 2021). Regulated local kinase signaling is a critical interface linking epileptic seizure susceptibility to learning/memory abilities (Cole, 2000; Wang and Chen, 2019). Major players are serine/threonine kinases protein kinase A (PKA) and extracellular signal-regulated kinase (ERK; Wiegert and Bading, 2011; Giese and Mizuno, 2013; Lee, 2015). PKA signaling is critical for circuit plasticity underlying learning and memory (Li et al., 1996; Blitzer et al., 1998). ERK signaling likewise contributes to synaptic plasticity (Impey et al., 1999; Mao and Wang, 2016). Their interactive signaling is complex, since cAMP activates both PKA and ERK, and PKA moreover activates and suppresses ERK function in a context-dependent manner (Wiegert and Bading, 2011; Taylor et al., 2013; Jain et al., 2018). This localized signaling integration drives the need to understand kinase function in baseline, activity-modulated, and disease model states. In particular, we need to determine when and where kinase signaling occurs in well-mapped brain learning/memory circuits. Knowledge of circuit-localized, subcellular kinase signaling is essential to instruct analyses of normal plasticity mechanisms and to improve dysfunction intervention strategies. To this end, we use transgenic kinase function biosensors to image localized signaling integration.

The *Drosophila* central brain mushroom body learning/memory center provides a model to dissect circuit-localized kinase signaling. This ∼2,000 Kenyon cell (KC) centered circuit (Aso et al., 2014b; Li et al., 2020; Modi et al., 2020) displays sensory-behavior integration plasticity requiring PKA and ERK signaling (Zhang et al., 2018b; Turrel et al., 2020; Zhao et al., 2023). Three KC classes (α/β, α'/β', γ) project to connectivity nodes of opposing behaviors (e.g., approach vs avoid; Crittenden et al., 1998; Aso et al., 2014a,b), with immunologically separable somata, calyx and axonal lobes (Liu et al., 2019; Lai et al., 2022). Defined KC classes have autonomous learning/memory roles, which require differential kinase signaling (Zars et al., 2000; Buchanan and Davis, 2010). For imaging, separation of phases-based activity reporter of kinase (SPARK) biosensors can be neuron-targeted for precise spatiotemporal analyses (Zhang et al., 2018a; Li et al., 2022). We previously mapped age-dependent PKA signaling to show normal function detectable in only three α'/β' output regions (α'1, β'1, β'2), but expanded by KC synaptic output blockade (Sears and Broadie, 2022). This PKA signaling plasticity begs the question of activity regulation in orchestration with ERK signaling, given the complex synergistic and antagonistic PKA/ERK signaling interactions (Wiegert and Bading, 2011; Taylor et al., 2013; Jain et al., 2018). We now use an ERK-SPARK biosensor to image signaling in both normal and activity-modulated circuits. We then image both PKA and ERK signaling in altered behavioral state models of enhanced learning/memory and elevated epileptic seizure susceptibility.

In this study, we first use SPARK reporters to image circuit-localized PKA and ERK signaling in resting, activity-modulated, and neurotransmission output-blocked conditions. We discover baseline distinctions between heightened PKA and ERK signaling domains, with heightened activity driving elevated function and newly-induced signaling domains. Kenyon cell neurotransmission blockade with targeted tetanus toxin (Doll et al., 2017) or temperature-sensitive dynamin (*shibire^{ts}*; Vijayakrishnan et al., 2010) broadens kinase signaling in both pre- and postsynaptic compartments. Potentiated circuit activity with transgenic sodium channels (NaChBac; Mabuchi et al., 2023) or temperature-sensitive TRP channels (TRPA; Dear et al., 2017) upregulates separable PKA and ERK signaling. We next employ SPARK reporters to image circuit-localized PKA and ERK signaling in behavioral mutant models improving learning/memory capabilities and elevating seizure susceptibility. Targeted Meng-Po kinase overexpression strengthening learning/memory (Lee et al., 2018) causes increased PKA and ERK signaling in distinct circuit connectivity nodes. The "bang-sensitive" *easily shocked* mutant epilepsy model (Jeong et al., 2021) consistently manifests elevated PKA and ERK signaling in nonoverlapping circuit domains. These results indicate coordinated PKA and ERK signaling at baseline with activity-dependent changes suggesting an untapped kinase potential associated with improved learning and memory.

Materials and Methods

Materials availability. Contact the senior author for assistance in obtaining any materials used in this study. We are pleased to share *Drosophila* lines with only reasonable compensation for shipping.

Data availability. All data supporting findings of this study are available from the senior author on request.

Drosophila *genetics.* All animals were reared and maintained on a 12/12 h light/dark cycle at 25°C with standard cornmeal/agar/molasses food, unless specified otherwise. Females and males were used in all experiments, unless specified otherwise. Animals were outcrossed to the *w^{1118}* genetic background control (Bloomington *Drosophila* Stock Center, BDSC 3605). The Kenyon cell OK107-Gal4 driver (BDSC 854; Connolly et al., 1996) was used with UAS-PKA-SPARK and UAS-ERK-SPARK to image circuit kinase signaling (Xiaokun Shu; Zhang et al., 2018a). The following UAS lines were used; (1) UAS-*Raf^{gof}* (BDSC 2033; Brand and Perrimon, 1994) and UAS-*rl^{Sem}* (BDSC 59006) to modulate ERK signaling (Brunner et al., 1994; Sun et al., 2020), (2) UAS-TNT with inactive UAS-IMP-TNT control (BDSC 28841; Brian McCabe, Brain Mind Institute, EPFL) (Yamasaki et al., 1994; Sweeney et al., 1995; Haag et al., 2016) and UAS-*shibire^{ts}* (BDSC 44222; Kitamoto, 2001) to block neurotransmission (Vijayakrishnan et al., 2010; Sears and Broadie, 2022), (3) UAS-NaChBac (BDSC 9469; Nitabach et al., 2006) and UAS-TRPA1 (BDSC #26263; Pulver et al., 2009) to elevate circuit activity (Dear et al., 2017), and (4) UAS-*meng-po.HA* (BDSC 80145; Lee et al., 2018) for overexpression. A *rolled* hypomorphic allele *rl^{1}* was used as an ERK loss of function control (BDSC 386; Biggs et al., 1994). The *easily shocked* (*eas^{2}*) allele was used as the hyperexcitable seizure model (Barry Ganetzky, University of Wisconsin; Benzer, 1971; Pavlidis et al., 1994; Pascual et al., 2005). X chromosome hemizygotic male *eas^{2}* mutants and matched controls were compared. UAS-SPARK animals were assayed alone or crossed with OK107-Gal4, for both UAS transgene and driver controls, respectively. In all experiments, the Gal4 driver and UAS responder(s) were always heterozygous (e.g., UAS-ERK-SPARK/+; OK107-Gal4/+).

Temporal thermogenetics. For conditional experiments, temperature-sensitive (ts) transgenes were used with timed temperature shifts as previously reported (Dear et al., 2017; Sears and Broadie, 2022). Briefly, UAS-*shibire^{ts}* is a dynamin semi-dominant negative above 29°C (Koenig et al., 1983; Kitamoto, 2001) to block synaptic transmission (Rohrbough and Broadie, 2002; Vijayakrishnan et al., 2010), and UAS-TRPA1 (transient receptor potential A1) is a cation channel activated above 23°C (Hamada et al., 2008; Pulver et al., 2009) to elevate neuronal function (Dear et al., 2017). UAS-SPARK; OK107-Gal4 animals were crossed with UAS-*shibire^{ts}* or UAS-TRPA1. Animals of all genotypes were reared at 20°C as eggs, larvae, and pupae until posteclosion. Adults were maintained at 20°C or moved to 30°C for 7 d. Animals maintained at 20°C as adults serve as controls, since 20°C is below dominant-

negative *shibire*^{ts} and TRPA1 channel activation thresholds. Adults at 30°C are the experimental groups. Age-matched control and experimental brains were processed in parallel for immunolabeling analyses as detailed below.

Immunocytochemistry imaging. *Drosophila* brains were dissected in phosphate-buffered saline (PBS) and then fixed for 10 min in 4% paraformaldehyde in PBS+ 4% sucrose with rotation at room temperature (RT). Brains were blocked for 1.5 h at RT with rotation in blocking buffer (PBS, 1% bovine serum albumin, 0.5% goat serum, 0.2% Triton X-100). Brains were incubated in a 1:100 dilution of mouse anti-Trio (DSHB 9.4A) in blocking buffer for 2 h at RT with rotation then washed three times for 10 min with blocking buffer. Brains were incubated with fluorescent secondaries and primaries for 2 h at RT with rotation, then washed three times for 10 min with blocking buffer. Brains were mounted between two #1 coverslips separated by a die-cut Oracal 651 vinyl spacer to allow for imaging of rostral (lobes) and caudal (somata and calyx) regions from each brain, with imaging performed from both directions. FITC-conjugated goat anti-GFP (Abcam ab6662; 1:500 dilution) was used to better visualize PKA-SPARK. Anti-mouse Alexa 555 (Invitrogen A31570; 1:500 dilution) was used to visualize Trio immunolabeling. Brightness and contrast were altered only in the case of Trio immunolabeling in figure images, with all changes to the entire image, to better display Trio+ and Trio− areas. Brains were imaged using confocal microscopy in serial optical sections as rostral lobe z-stacks and caudal calyx/somata z-stacks. The focal planes, sections, and stacks shown are indicated in all figure legends. Mounted brains were imaged using an LSM 510 Zeiss confocal microscope and a PLAN Apochromat 63X/1.4NA objective, with pixel dwell of 1.26 µs and 1 µm optical slice width as z stacks of rostral lobes and caudal somata + calyx.

Experimental design and statistical analysis. Animals were reared as described above with molecular genetics enabling expression of SPARK tools in the Kenyon cells in aged *Drosophila* adult brains. Brains were extracted, processed, and imaged using confocal microscopy in serial optical sections. SPARK puncta were counted using the ImageJ Point Tool and circuit localized using established mushroom body output neuron (MBON) maps (Tanaka et al., 2008; Aso et al., 2014b). Neuron classes were identified using Trio immunolabeling, which labels γ neurons moderately, α'/β' neurons strongly, and does not label α/β neurons (Liu et al., 2019; Lai et al., 2022). Cells and lobes were separated during analysis by location, position, labeling, and z-stack depth. All statistical analyses were conducted using GraphPad Prism (version 10). Datasets were compared using either two-tailed Mann–Whitney tests ($n = 2$ datasets) or with Kruskal–Wallis tests with Dunn's correction ($n > 2$ datasets). All graphs display individual data points and mean ± SEM. Significance is shown as $^{*}p < 0.05$, $^{**}p < 0.01$, $^{***}p < 0.001$ and is not statistically significant ($p > 0.05$; n.s.).

Results

Differential circuit-localized PKA and ERK signaling in Kenyon cells

We began by testing side-by-side PKA and ERK signaling in Kenyon cells (KCs). The three major classes (α/β, α'/β', γ) extend dendrites into the calyx, and axons into five lobes (α, β, α', β',γ; Tanaka et al., 2008; Aso et al., 2014b; Modi et al., 2020). Other KC classes, dorsal γ (γd) and α/βp, project to near lobe regions and adjacent ventral/dorsal accessory calyx, respectively (Aso et al., 2014b). The lobes are subdivided into 16 tiling domains (e.g., α'1, β'1, β2, α3, γ1, γ3, γ5) with informed circuit signaling maps (Aso et al., 2014b; Sears and Broadie, 2022). Kenyon cells project to both aversive and appetitive outputs, making them powerful models to analyze compartmentalized kinase signaling (Aso et al., 2014a; Modi et al., 2020; Davis, 2023). Kenyon cells display variable baseline excitability, with α'/β' showing higher excitability (Turner et al., 2008; Inada et al., 2017; Leinwand and Scott, 2021). To test PKA and ERK signaling, we use Kenyon cell OK107-Gal4 (Connolly et al., 1996; Pardo-Garcia et al., 2023) to drive the two SPARK biosensors which, when phosphorylated by each specific kinase, reversibly generate florescent GFP puncta (Zhang et al., 2018a; Sears and Broadie, 2020; Shaheen et al., 2023). Since the two SPARK biosensors have different fluorescence labels, affinities, and EC_{50} levels (Zhang et al., 2018a), we cannot compare their quantification directly. However, we can compare circuit domains with/without detectable signaling, as well as altered signaling from experimental manipulations. All imaging is staged at 7 d posteclosion (7 dpe, 25°C) to reduce result variation. To lay the groundwork for subsequent activity-modulated conditions, mutant analyses, and behavioral models, we start by testing side-by-side PKA and ERK signaling in the resting (basal) ground state.

We previously found baseline PKA signaling to be upregulated in only 3 of the 16 axon lobe domains (α'1, β'1, and β'2), with few PKA-SPARK puncta present outside these defined connectivity nodes (Sears and Broadie, 2022). In sharp contrast, heightened ERK signaling is restricted primarily to the α and β lobes, especially to α3 and β2 domains (Fig. 1*A*, top rows). Importantly, ERK-SPARK puncta are not detected in the α'1, β'1, and β'2 output domains, where PKA signaling predominates. Quantification shows high PKA-SPARK and low ERK-SPARK puncta in both the α'1 and β'1 circuit nodes, with significant ($p = 0.000000740$; Mann–Whitney $U = 0$), >50-fold elevated PKA-SPARK puncta over ERK-SPARK puncta in both these domains (Fig. 1*B*, left). Conversely, there is undetectable PKA-SPARK puncta and extremely high ERK-SPARK puncta in both the α3 and β2 nodes, with significant ($p = 0.000000740$; Mann–Whitney $U = 0$), >45-fold elevation of ERK-SPARK over PKA-SPARK puncta (Fig. 1*B*, right). As will become important later in these analyses, neither PKA nor ERK biosensors detect any significant baseline signaling in the medial γ lobe (γ2 to γ5; Fig. 1*A*, top and 2nd rows). Thus, in the resting, basal state, heightened PKA and ERK signaling is circuit-localized to a small subset of Kenyon cell output domains, with a striking presynaptic separation between PKA (α'/β') and ERK (α/β) signaling. We conclude that this spatial distinction indicates independent regulation and the possibility of antagonistic regulatory interactions.

We next sought to test other circuit regions for distinguishable kinase signaling, including Kenyon cell somata and mushroom body calyx dendritic arbors. Axonal lobes are easily mapped based on their distinctive architecture, but delineating somata and calyx regions is much more difficult. We therefore co-labeled with an antibody against the RhoGEF Trio, which clearly marks γ and α'/β' neurons, with no α/β labeling (Liu et al., 2019; Lai et al., 2022). PKA signaling occurs in both Trio negative (Trio−) and Trio positive (Trio+) somata, with more PKA-SPARK puncta in Trio− cells (Fig. 1*A*, somata). In direct contrast, there are almost no detectable ERK-SPARK puncta in the somata (Fig. 1*C*). Quantification shows high PKA-SPARK puncta in the Trio− somata, with a significant ($p = 0.000175$; Mann–Whitney $U = 0$), >30-fold elevation over ERK-SPARK puncta number (Fig. 1*C*). In the calyx, PKA signaling is elevated in the Trio+ regions, but not in the Trio− negative regions (Fig. 1*A*, bottom, yellow dashed circles). ERK-SPARK puncta are nearly undetectable in the calyx (Fig. 1*D*). Quantification shows high PKA signaling in Trio+ calyx regions, and higher overall PKA-SPARK compared to ERK-SPARK puncta ($p = 0.000175$; Mann–Whitney $U = 0$; >60-fold difference; Fig. 1*D*). To test for leaky expression, we compared both PKA- and ERK-SPARK, with and without the OK107-Gal4

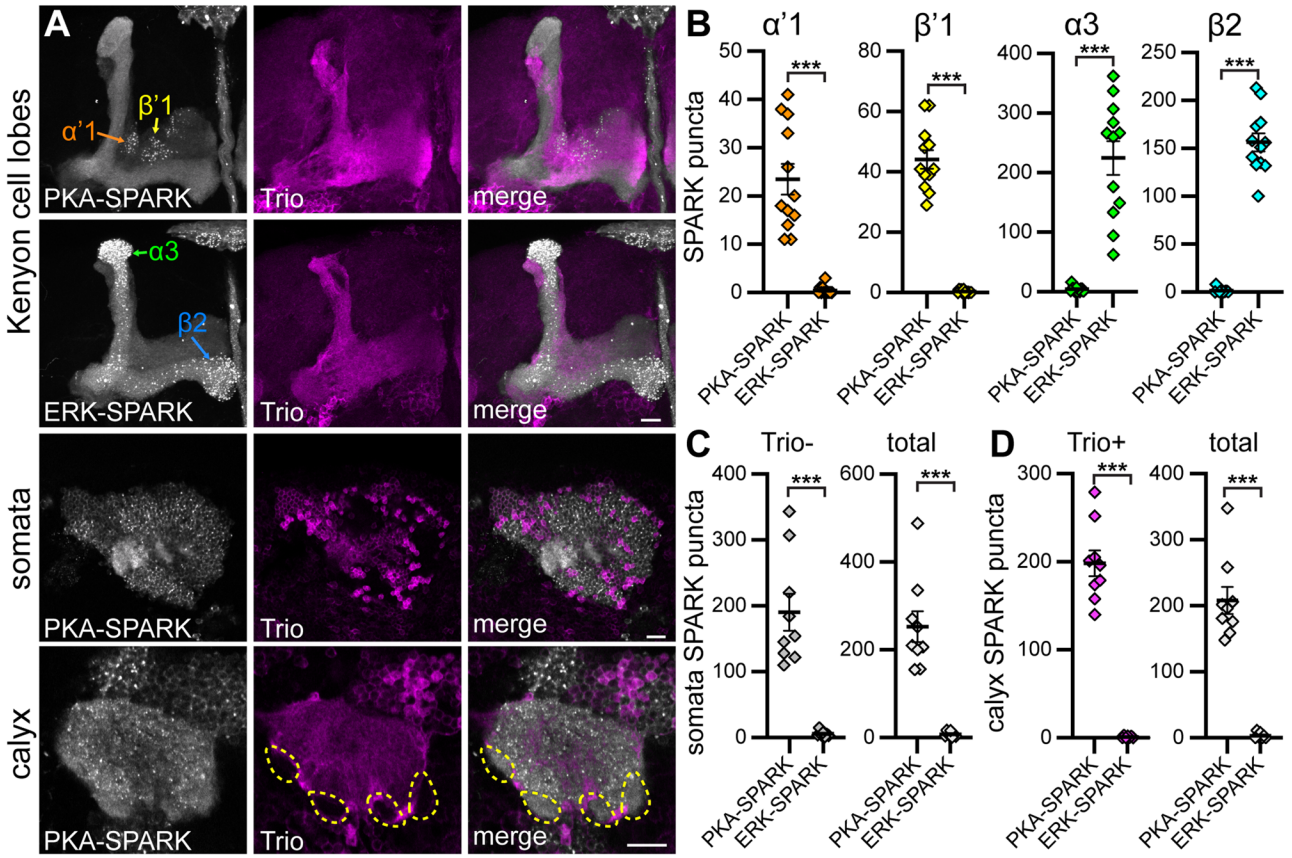

Figure 1. Distinct PKA versus ERK signaling in Kenyon cell connectivity nodes. ***A***, *Drosophila* brain imaging of PKA-SPARK and ERK-SPARK signaling (grayscale) with the OK107-Gal4 driver for Kenyon cells in the mushroom body learning/memory center. Co-labeled with anti-Trio (magenta), with the merged images on the right. Highlighted are the axonal lobes (top), Kenyon cell somata (middle) and dendritic arbor calyx (bottom). Dashed yellow lines delineate Trio—negative calyx regions. ***B***, Quantification of SPARK puncta in indicated lobe circuit nodes. ***C***, Quantification of SPARK puncta in Kenyon cell somata. ***D***, Quantification of SPARK puncta in the calyx. Trio-positive (Trio+), negative (Trio—) and total domain counts are shown as indicated. Images are z-projections (lobes) or single slices (somata and calyx), with the lobes in rostral and calyx/somata in caudal aspects of the brain. All individual data points shown with mean ± SEM. Significance in Mann–Whitney tests: ***$p < 0.001$. Scale bars: 10 µm.

driver. We find detectable SPARK expression only if OK107-Gal4 is present (Fig. 2). Taken together, we find higher PKA signaling but negligible ERK signaling in Kenyon cell somata, and similarly higher PKA signaling especially in Trio+ regions of the postsynaptic calyx, but nominal ERK signaling in the calyx. We next turned to dissecting this newly revealed localized ERK signaling in the Kenyon cell circuit.

Distinct circuit-localized ERK signaling with layered pathway activation

ERK signaling has been previously reported to show activity-dependent induction, but circuit mapping of ERK signaling with immunolabeling alone is extremely challenging (von Kriegsheim et al., 2009; Zhang et al., 2018b). To test the regulation of the above ERK-SPARK signaling within Kenyon cells, we used two targeted pathway manipulations; (1) a constitutively active gain-of-function Raf (Raf^{gof}) upstream in the mitogen-activated protein kinase (MAPK) regulatory pathway (Brand and Perrimon, 1994; Wei et al., 2021) and (2) constitutively active $Rolled^{Sevenmaker}$ (Rl^{Sem}) directly at the level of ERK enzymatic function (Brunner et al., 1994; Sun et al., 2020). With these two OK107-Gal4 targeted transgenic manipulations, we fully expected maximally elevated ERK-SPARK signaling throughout the Kenyon cells, as we reported previously for transgenic PKA-C activation of PKA-SPARK signaling (Sears et al., 2019; Sears and Broadie, 2020). However, to our surprise, both Raf^{gof} and Rl^{Sem} drive elevated ERK-SPARK signaling to a more limited degree (Fig. 3), suggesting very strong restrictive mechanisms must exist in Kenyon cells to limit ERK signaling activation. Using the same circuit mapping strategy as above, we test localized ERK-SPARK signaling induced by pathway activation at these two very different levels (Raf^{gof} and Rl^{Sem}) compared to the OK107-Gal4 transgenic driver control. We assay ERK-SPARK signaling in all three genotypes in the mapped Kenyon cell lobe presynaptic domains, somata, and calyx postsynaptic dendritic arbors. Representative images and quantified results are shown in Figure 3.

Compared to the driver control, Raf^{gof} and Rl^{Sem} increase ERK signaling within the α/β lobes (Fig. 3*A*). Quantification shows significant elevations in β2 for Raf^{gof} and Rl^{Sem} (control vs Raf^{gof}, $p = 0.0436$, $Z = 2.29$; control vs Rl^{Sem}, $p = 0.000714$, $Z = 3.57$; Fig. 3*B*, left). Interestingly, Raf^{gof} but not Rl^{Sem} drives expanded ERK signaling in two medial domains; γ5 and dorsal γ5 (Fig. 3*A*). Quantification reveals significant increases in both domains (γ5, control vs Raf^{gof}, $p = 0.000139$, $Z = 3.98$; γ5, control vs Rl^{Sem}, $p = 0.999$, $Z = 0.263$; dorsal γ5, control vs Raf^{gof}, $p = 0.000373$, $Z = 3.737$; control vs Rl^{Sem}, $p = 0.999$, $Z = 0.465$; Fig. 3*B*, center/right). In Kenyon cell somata, ERK signaling is elevated with both Raf^{gof} and Rl^{Sem} (Fig. 3*C*). Raf^{gof} results in stronger activation, with enlarged ERK-SPARK puncta relative to Rl^{Sem}. Trio immunolabeling reveals further striking differences; Raf^{gof} causes elevated ERK signaling almost exclusively within the Trio+ neurons, whereas Rl^{Sem} drives ERK signaling

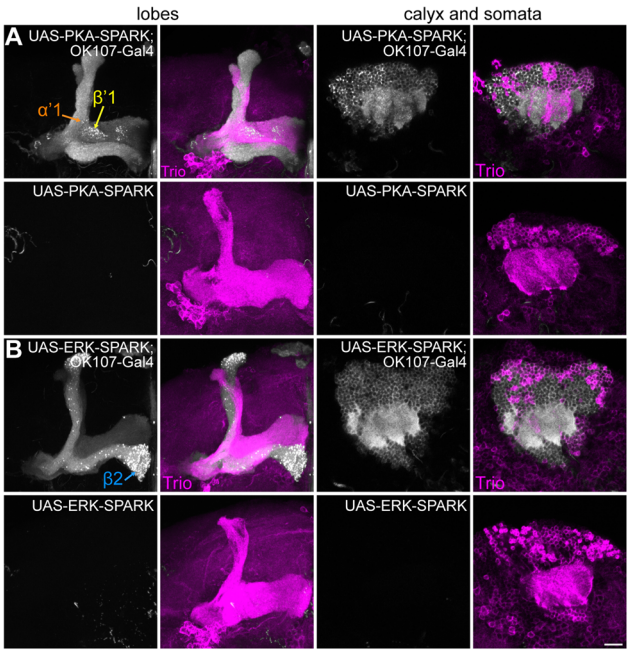

Figure 2. PKA- and ERK-SPARK biosensors require Kenyon cell driver expression. ***A***, The UAS-PKA-SPARK biosensor driven by the Kenyon cell OK107-Gal4 driver (top) and without the driver (bottom). Images are separated to show the mushroom body axonal lobes (left) and the postsynaptic calyx with somata (right). The PKA-SPARK signal alone is displayed in grayscale (first and third columns), and together with anti-Trio (magenta) co-labeling (second and fourth columns). There is no detectable PKA-SPARK in the absence of the driver. ***B***, UAS-ERK-SPARK biosensor imaging displayed in an identical manner. Note the Kenyon cell circuit domain separation between PKA signaling (***A***) and matched ERK signaling (***B***). There is no detectable ERK-SPARK in the absence of the Kenyon cell OK107-Gal4 driver, showing targeted biosensor reporting. All images shown are z-stack projections of lobes or single slice somata/calyx. Scale bar: 10 µm.

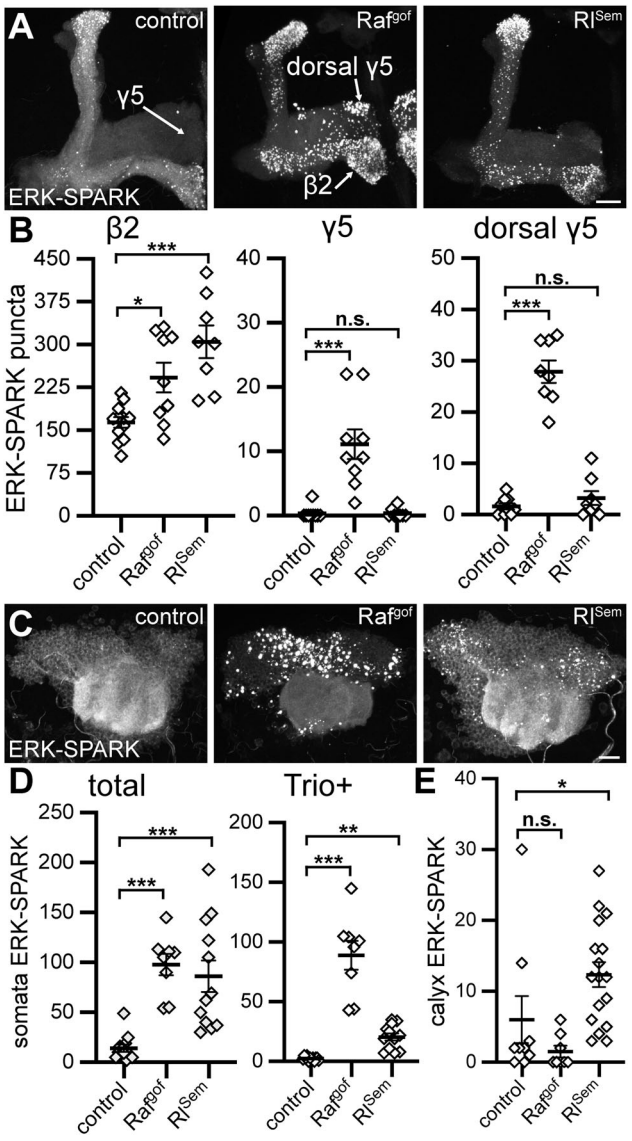

Figure 3. Localized ERK signaling with gain-of-function ERK pathway activation. ***A***, ERK-SPARK in Kenyon cell axonal lobes in the OK107-Gal4 driver control (left), and driving UAS-Raf^{gof} (middle) and UAS-ERK/RI^{Sem} (right). The circuit connectivity nodes with the largest ERK signaling changes are indicated. ***B***, Quantification of ERK-SPARK puncta within the indicated lobe nodes. ***C***, ERK-SPARK within the Kenyon cell somata and adjacent postsynaptic calyx with the OK107-Gal4 driver control (left) and driving UAS-Raf^{gof} (middle) and UAS-ERK/RI^{Sem} (right). Quantification of ERK-SPARK puncta in somata (***D***) and in the calyx dendritic arbor (***E***). All images are z-stack projections, with lobes in rostral and calyx/somata in caudal aspects of the brain. All individual data points shown with mean ± SEM. Significance in Kruskal–Wallis tests with Dunn's correction: $^{*}p < 0.05$, $^{**}p < 0.01$, $^{***}p < 0.001$, and not statistically significant (n.s.). Scale bars: 10 µm.

in Trio+ and Trio− somata (Fig. 3*C*). Quantification shows a significant increase in ERK-SPARK puncta in the Kenyon cell somata with both Raf^{gof} and RI^{Sem} (control vs Raf^{gof}, $p = 0.000146$, $Z = 3.97$; control vs RI^{Sem}, $p = 0.000319$, $Z = 3.78$; >5-fold difference; Fig. 3*D*). Within the postsynaptic calyx, we observe only weak ERK signaling activation with RI^{Sem}, and none at all with Raf^{gof} (Fig. 3*C*). Quantification shows a small but significant increase of ERK-SPARK puncta with RI^{Sem} (control vs RI^{Sem}, $p = 0.0223$, $Z = 2.54$; Fig. 3*E*). Taken together, both Raf^{gof} and RI^{Sem} drive circuit-localized ERK signaling, in overlapping as well as different cell types, perhaps due to downstream regulation. Given the strong Raf^{gof} phenotype, we next tested ERK function by introducing the viable *rolled*/ERK hypomorph *rl*^{1}.

We first compared *rl*^{1} homozygous mutants to matched controls with ERK-SPARK expressed in the Kenyon cells (Fig. 4*A*,*B*). Consistent with expectations, we find *rl*^{1} mutants display far fewer ERK-SPARK puncta in α/β domains of normally heightened ERK signaling (Fig. 4*A*). To quantify this phenotype, we assayed both β1 and β2 (Fig. 4*A*, left) to find significant reduction in ERK-SPARK puncta in *rl*^{1} mutants in both domains (β1: $p = 0.0000289$, Mann–Whitney $U = 29.5$; β2: $p = 0.00000585$, Mann–Whitney $U = 22$; Fig. 4*B*). We next compared animals expressing Raf^{gof} in Kenyon cells with animals in a *rl*^{1} homozygous mutant background (*rl*^{1}; Raf^{gof}). These double mutants show suppression of Raf^{gof}-dependent ERK-SPARK puncta, with a signaling loss in both γ5 and dorsal γ5 compared to Raf^{gof} alone (Fig. 4*C*). Quantification reveals a highly significant decrease in ERK-SPARK puncta in both domains in *rl*^{1}; Raf^{gof} double mutants compared to Raf^{gof} animals (γ5: $p = 0.000382$, Mann–Whitney $U = 23$; dorsal γ5: $p = 0.000000598$, Mann–Whitney $U = 3$; Fig. 4*D*). Finally, we predicted the *rl*^{1} background would prevent Raf^{gof}-dependent ERK-SPARK puncta signaling in Trio+ somata (Fig. 3). Consistently, we find an almost total loss of ERK-SPARK puncta in the Kenyon cell somata of Raf^{gof} in the *rl*^{1} mutant background (Fig. 4*E*). There is a large reduction in ERK-SPARK puncta in the somata ($p = 0.00000231$, Mann–Whitney $U = 4$), with the most ERK signaling loss in Trio+ somata (Fig. 4*F*). Taken together, we find *rl*^{1} mutants have ERK-SPARK puncta loss both at baseline and with Raf^{gof}

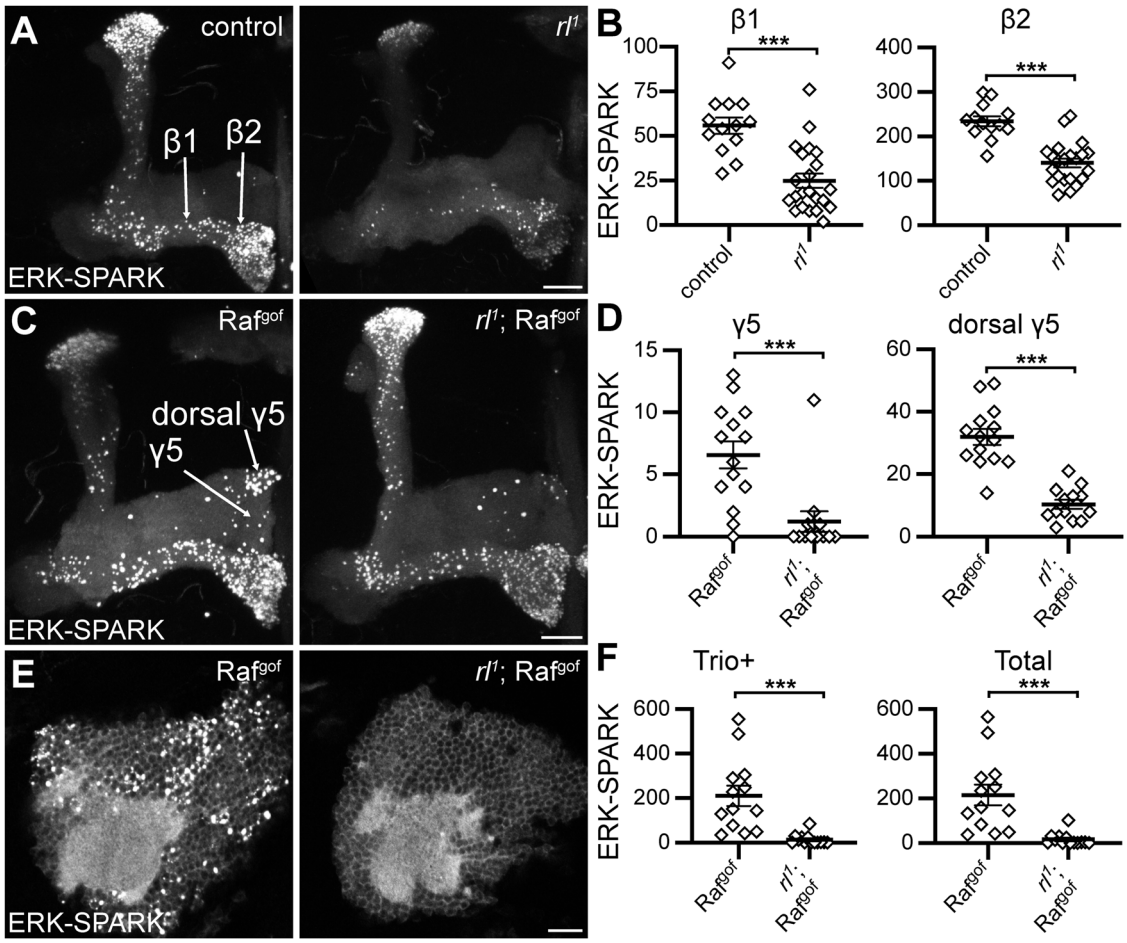

Figure 4. ERK reduction lowers baseline and Raf^{gof}-dependent ERK signaling. ***A***, ERK-SPARK in Kenyon cell axonal lobes driven by OK107-Gal4 in control animals (left) and in the homozygous *rl*^{1} hypomorphic mutant in ERK (right). ***B***, Quantification of ERK-SPARK puncta within the indicated compartments. ***C***, ERK-SPARK in Kenyon cell axonal lobes with OK107-Gal4 driven UAS-Raf^{gof} in the control background (left), and in the *rl*^{1} mutant background (right). ***D***, Quantification of ERK-SPARK puncta within the indicated compartments. ***E***, ERK-SPARK in Kenyon cell somata and calyx with OK107-Gal4 driven UAS-Raf^{gof} in the control background (left), and in the *rl*^{1} mutant background (right). ***F***, Quantification of ERK-SPARK puncta in Trio+ somata (left) and in all somata (right). Images are z-projections (lobes) or single slices (somata and calyx), with lobes in rostral and calyx/somata in caudal aspects of the brain. All individual data points shown with mean ± SEM. Significance in Mann–Whitney tests: ***$p < 0.001$. Scale bars: 10 µm.

activation. We next turned to circuit signaling as a mechanism for this ERK pathway regulatory control.

Targeted neurotransmission blockade elevates localized ERK signaling

Kenyon cell neurotransmission output provides both lateral control and feedback regulation via compartmentalized PKA signaling (Manoim et al., 2022; Sears and Broadie, 2022). To test impacts on circuit-localized ERK signaling, we first use targeted tetanus toxin light chain (TNT) to block Kenyon cell synaptic transmission (Sweeney et al., 1995; Haag et al., 2016). TNT proteolytically cleaves the vesicle SNARE Synaptobrevin to prevent synaptic vesicle exocytosis fusion (Link et al., 1992; Schiavo et al., 1992). We use Kenyon cell OK107-Gal4 to target ERK-SPARK and quantify puncta with TNT block, without TNT, and with a mutated inactivated IMP-TNT control (Yamasaki et al., 1994). In the axonal lobes, ERK signaling is relatively normal in the absence of neurotransmission, with one dramatic exception; TNT causes profound ERK signaling induction in the core γ1 domain stretching deep into the anterior pedunculus (Fig. 5*A*). This γ1 output node sub-region is composed of Trio− α/β neurons, suggesting that circuit output limits signaling in this specific domain. 3D-projections reveal the striking TNT neurotransmission block expansion (Fig. 5*A*, lower panels). Quantification shows few γ1 ERK-SPARK puncta in background and IMP-TNT controls, but a significant, >4-fold puncta increase with the TNT blockade (control vs IMP-TNT, $p = 0.896$, $Z = 1.04$; control vs TNT, $p = 0.00000281$, $Z = 4.90$; IMP-TNT vs TNT, $p = 0.00000321$, $Z = 4.88$; Fig. 5*B*). A loss of Kenyon cell synaptic function also causes expansion of postsynaptic ERK signaling within the calyx (Fig. 5*C*). Quantification in the calyx once again shows few ERK-SPARK puncta in background and IMP-TNT controls, but a significant, >5-fold increase with TNT blockade (control vs IMP-TNT, $p = 0.999$, $Z = 0.677$; control vs TNT, $p = 0.00233$, $Z = 3.36$; IMP-TNT vs TNT, $p = 0.00000283$, $Z = 4.90$; Fig. 5*D*).

To further test the role of KC synaptic output regulation on local ERK signaling, independent of possible developmental effects, we used a targeted, conditional method to block neurotransmission. The temperature-sensitive (ts) mutation in dynamin (*shibire*^{ts}) blocks synaptic vesicle cycling to completely prevent neurotransmission at temperatures above 29°C (Koenig et al., 1983; Kitamoto, 2001). We used the OK107-Gal4 driver to target *shibire*^{ts} to Kenyon cells, and tested ERK-SPARK signaling at permissive (20°C) and restrictive (30°C) temperatures. We previously reported similar neurotransmission blockade phenotypes for

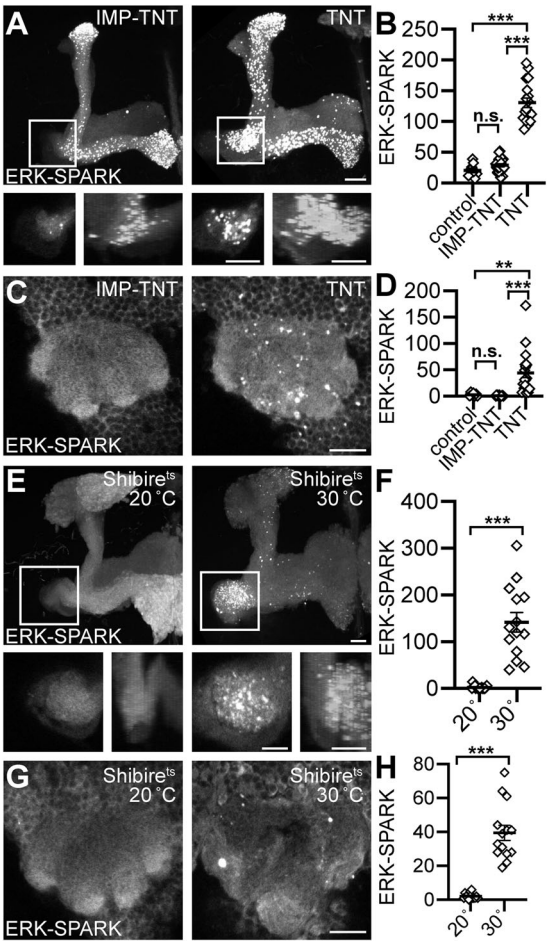

Figure 5. Expanded ERK signaling with synaptic transmission output blockade. ***A***, ERK-SPARK imaging in the axonal lobes with inactive tetanus toxin control (IMP-TNT; left) and tetanus toxin light (TNT; right) to block Kenyon cell synaptic output. Upper panel boxed areas displayed below at higher magnification, as single slices (left) and 90° rotated 3D-projections (right). ***B***, ERK-SPARK quantification in boxed domains. ***C***, ERK-SPARK in the calyx under the same conditions. ***D***, ERK-SPARK puncta quantification in calyxes. ***E***, ERK-SPARK imaging in the axonal lobes with *shibire*^{ts} at permissive 20°C (left) and restrictive 30°C (right) to block Kenyon cell synaptic output. Images displayed identically to (***A***). ***F***, ERK-SPARK quantification in boxed domains. ***G***, ERK-SPARK in the calyx under the same conditions as (***E***). ***H***, Quantification of ERK-SPARK puncta in the calyx. Z-projections (lobes), 3D projections (indicated above), or single slices (calyx and as indicated above) are shown, with lobes in rostral and calyx/somata in caudal aspects of the brain, and γ1/pedunculus caudal relative to other lobe regions. All individual data points shown with mean ± SEM. Significance from Kruskal–Wallis tests with Dunn's correction (***B,D***) or Mann–Whitney tests (***F,H***): $^{**}p < 0.01$, $^{***}p < 0.001$, and not statistically significant (n.s.). Scale bars: 10 µm.

TNT and *shibire*^{ts} in the regulation of PKA-SPARK signaling (Sears and Broadie, 2022), although we also observed mushroom body morphological defects in *shibire*^{ts} mutants even at permissive temperatures. Based on above TNT analyses, we predicted elevated ERK-SPARK signaling in the γ1 domain of adult *shibire*^{ts} mutants at the blockaded 30°C, relative to 20°C control. Consistently, compared to the permissive 20°C condition, we find a significant increase in γ1 ERK-SPARK at restrictive 30°C ($p = 0.00000000688$; Mann–Whitney $U = 0$; Fig. 5*E,F*). Also consistent with TNT results, we find significantly higher ERK-SPARK signaling in the calyx of adults at 30°C relative to the 20°C controls ($p = 0.0000000499$; Mann–Whitney $U = 0$; Fig. 5*G,H*). As reported previously (Sears and Broadie, 2022), we also observe *shibire*^{ts} mushroom body morphological defects at both 20°C and 30°C (Fig. 5*E,G*). These results indicate KC neurotransmission local feedback inhibition of ERK signaling. We next used targeted channel manipulations to test for activity-dependent kinase signaling alterations.

Potentiated circuit activity induces separable PKA and ERK signaling domains

The above results indicate that Kenyon cell circuit domains differentially regulate kinase activation. We hypothesized activity-dependent control with the local induction of PKA versus ERK signaling to drive kinase-specific activation patterns. To test this hypothesis, we drove the depolarization-activated NaChBac sodium channel in Kenyon cells, which acts to potentiate normal circuit activity, rather than imposing exogenous activity (Nitabach et al., 2006; Zimmerman et al., 2017). We used PKA- and ERK-SPARK biosensors, with analyses in both Kenyon cell presynaptic axonal lobes and postsynaptic calyx. With PKA-SPARK, we find NaChBac induces strong PKA signaling in the α/β lobes, including both the β2 and α2 nodes (Fig. 6*A*, left). Quantification reveals a significant ($p = 0.0000000575$; Mann–Whitney $U = 0$), >250-fold signaling induction in β2 compared to controls (Fig. 6*B*). In the anterior γ3 domain, we likewise find abundant PKA-SPARK puncta that are nearly absent in control animals (>70-fold difference; $p = 0.000000213$; Mann–Whitney $U = 0$). In the postsynaptic calyx, NaChBac activity expands PKA signaling in dendritic arbors, with densely-packed, large PKA-SPARK puncta in all calyx regions (Fig. 6*A*, right). Quantification shows a significant, >4-fold increase in PKA-SPARK puncta with elevated activity compared to the driver control ($p = 0.000311$, Mann–Whitney $U = 0$; Fig. 6*B*, right). We conclude that Kenyon cell activity strongly drives localized PKA signaling, with NaChBac channel-induced heighted activity expanding axonal lobe presynaptic signaling in both the α/β and γ3 connectivity nodes, as well as dramatically increasing the postsynaptic signaling within the calyx dendritic arbors.

For ERK-SPARK signaling, we again find low overall signaling in both α' and β' lobes, with clear ERK activation in both α and β connectivity nodes (Fig. 6*C*, left). Compared to the driver controls, NaChBac-potentiated activity causes elevated ERK signaling in a subset of lobe domains, with particularly strong induction in the γ5 node (Fig. 6*C*, lower left). However, note that ERK signaling is still absent in the β'1 domain (Fig. 6*C*, yellow arrow). Quantification shows a very high activity-dependent elevation in the number of ERK-SPARK puncta in the γ5 circuit domain compared to the controls, indicating a significant ($p = 0.0000119$; Mann–Whitney $U = 0$), >200-fold local increase in the ERK signaling level (Fig. 6*D*, left). In the postsynaptic calyx, the driver controls display few if any ERK-SPARK puncta, again demonstrating very low baseline ERK signaling (Fig. 6*C*, right). In sharp contrast, calyx regions with NaChBac-potentiated activity show a dramatic increase in the level of local ERK signaling, with especially dense concentrations of enlarged ERK-SPARK puncta within the Trio– α/β Kenyon cell dendritic arbors (Fig. 6*C*, dashed yellow lines). Quantification reveals a highly increased number of activated ERK-SPARK puncta within the postsynaptic calyx with NaChBac activity potentiation compared to the driver controls, which is a significant, >50-fold elevation in circuit-localized ERK signaling in these KC postsynaptic domains ($p = 0.000250$; Mann–Whitney $U = 0$; Fig. 6*D*, right).

To further explore the role of Kenyon cell activity regulation of kinase signaling, independent of possible developmental effects, we used a targeted, conditional method to induce elevated activity. The temperature-gated TRPA1 channel (Hamada et al., 2008;

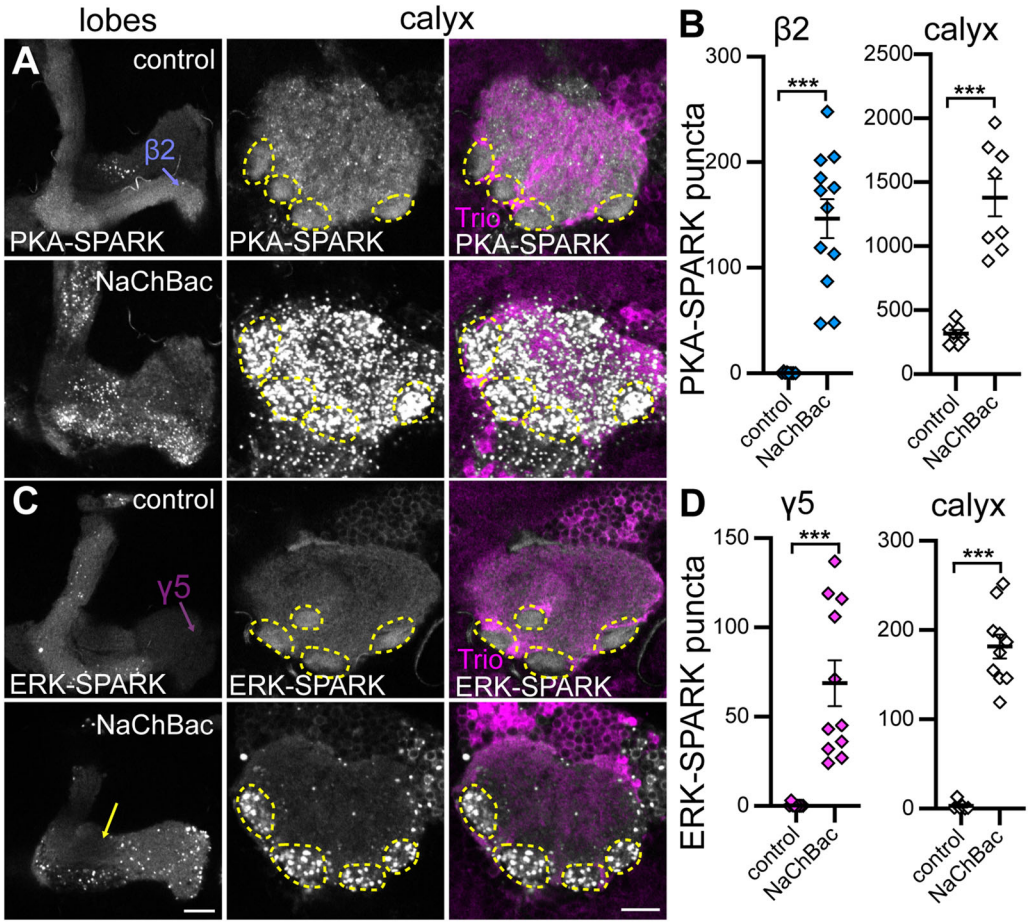

Figure 6. Potentiated activity induces circuit-localized PKA and ERK signaling. ***A***, PKA-SPARK imaging in the OK107-Gal4 driver control (top) or with expression of the voltage-gated Na^+ channel NaChBac (bottom) in Kenyon cell axonal lobes (left column) and postsynaptic calyx (middle column). Anti-Trio colabelling (magenta) is shown for the merged images (right column). Dashed yellow lines indicate the Trio-negative domains. ***B***, Quantification of PKA-SPARK puncta in the indicated domains. ***C***, ERK-SPARK imaging under identical conditions. The yellow arrow indicates the β′1 domain. Dashed yellow lines delineate the Trio-negative domains. ***D***, Quantification of ERK-SPARK puncta in the two indicated circuit domains. Images are single slices, with lobes in rostral and calyx in caudal aspects of the brain. All individual data points shown with mean ± SEM. Significance in Mann–Whitney tests: ***$p < 0.001$. Scale bars: 10 µm.

Pulver et al., 2009; Dear et al., 2017) allows for the temperature-dependent elevation in neuronal activity. At temperatures above 23°C, TRPA1 elicits strong neuronal activity and cause both striking and sustained behavioral effects (Pulver et al., 2009). As above, we used the OK107-Gal4 driver to target UAS-TRPA1 to Kenyon cells, and tested both the PKA-SPARK and ERK-SPARK signaling at the inactive control (20°C) and activity induced (30°C) temperatures. To eliminate possible developmental effects, we reared animals at 20°C until adulthood, then compared adults maintained at 20°C to adults shifted to 30°C. PKA-SPARK and ERK-SPARK signaling induction patterns at 30°C similar to NaChBac would support an activity-dependent regulatory mechanism. Like constitutive NaChBac, conditional adult TRPA1 expression with 30°C activation increases PKA-SPARK puncta in the β2, γ3, and calyx domains ($p = 0.000000000961$, Mann–Whitney U 3.5; $p = 0.00000000491$, Mann–Whitney $U = 6.5$; $p = 0.00124$, Mann–Whitney $U = 2$, respectively; Fig. 7*A*,*B*). Likewise, ERK-SPARK puncta are increased in both γ5 and the calyx ($p = 0.000108$, Mann–Whitney $U = 0$; $p = 0.00216$, Mann–Whitney $U = 0$, respectively; Fig. 7*C*,*D*). Taken together, these combined results reveal striking activity-dependent kinase signaling induction within tightly-restricted circuit domains.

Increased neuronal activity may alter output-dependent affects, or vice versa, so we next attempted to separate cell-autonomous functions by simultaneously driving both TNT and NaChBac together in Kenyon cells (Fig. 8). Using the OK107-Gal4 driver to express ERK-SPARK, we quantified signaling puncta in circuit-localized domains. Like NaChBac alone, we find significant ERK-SPARK induction in the γ5 domain and a lack of signaling in α'1 and β'1 domains (Fig. 8*A*). Quantification reveals a significant increase in γ5 ERK-SPARK puncta ($p = 0.0000457$, Mann–Whitney $U = 0$; Fig. 8*B*, left). Unlike TNT alone, we find ERK-SPARK puncta numbers in the γ1 inner domain comparable to driver control, and expanded signaling in the surrounding KC neuropil (Fig. 8*A*). Quantification reveals similar ERK-SPARK puncta in the γ1 inner domain comparing the driver controls to animals with both TNT and NaChBac ($p = 0.106$, Mann–Whitney $U = 32$; Fig. 8*B*), but also increased ERK signaling in the γ1 outer domain ($p = 0.00000313$, Mann–Whitney $U = 0$; Fig. 8*B*). IMP-TNT controls show a similar lack of ERK-SPARK puncta in outer γ1 compared to controls ($p = 0.278$, Mann–Whitney $U = 32.5$). However, defects/gaps in the α/β/γ neuropils complicate this interpretation, showing sensitivity to combined transgenic manipulation. These results suggest complex roles for KC synaptic output in the context of elevated neuronal activity, and feedback-independent signaling in circuit domains with activity-dependent regulation. We next turned to behavioral mutant

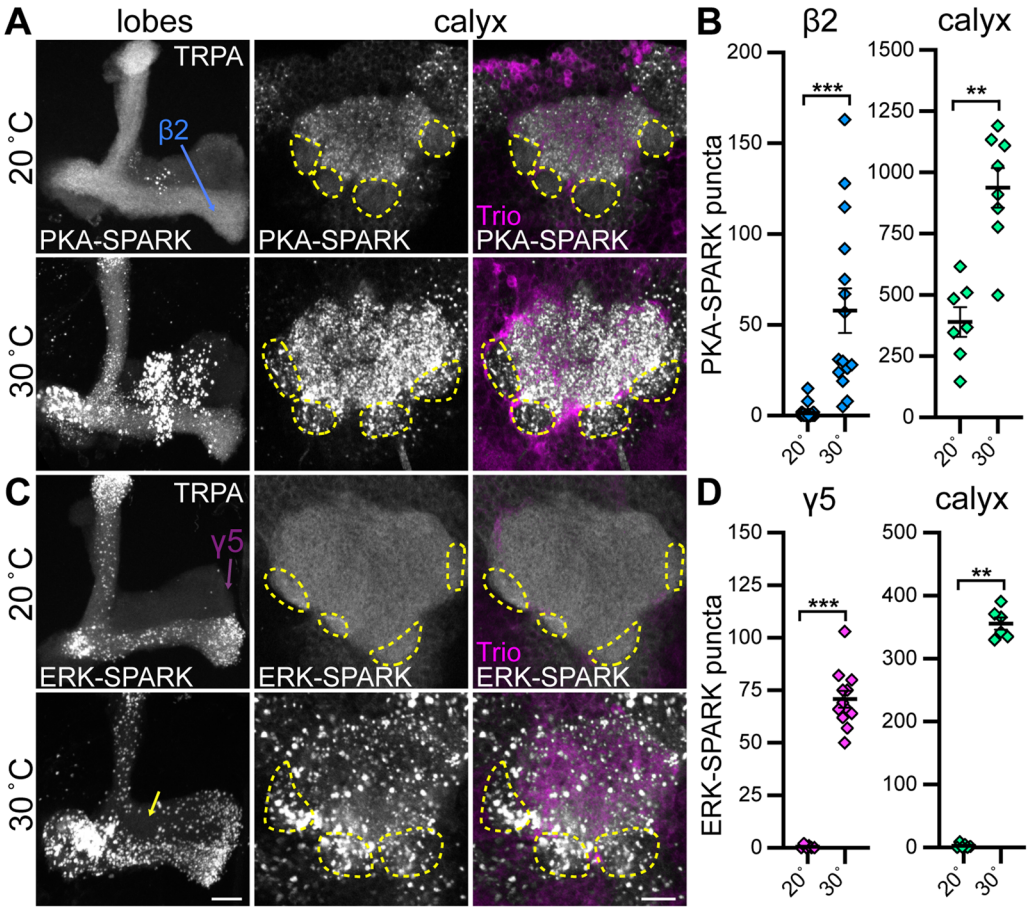

Figure 7. Thermogenetic activity induces circuit-localized PKA and ERK signaling. ***A***, PKA-SPARK imaging with OK107-Gal4 driving temperature-sensitive TRPA1 in axonal lobes (left), calyx (middle), and with anti-Trio (magenta) colabeling (right). Dashed yellow lines indicate Trio-negative domains. The control inactive temperature (20°C) is shown in the top panels, and channel-activating temperature (30°C) is shown in the bottom panels. ***B***, Quantification of PKA-SPARK puncta in indicated circuit domains. ***C***, ERK-SPARK imaging under identical conditions as (***A***). The yellow arrow indicates β′1. Dashed yellow lines delineate Trio-negative domains. ***D***, Quantification of ERK-SPARK puncta in the two indicated circuit domains. Images are z-projections (lobes) or single slices (calyx). All individual data points shown with mean ± SEM. Significance from Mann–Whitney tests: $^{**}p < 0.005$ and $^{***}p < 0.001$. Scale bars: 10 µm.

models to test for associated circuit-localized kinase signaling changes.

Meng-Po/SBK1 overexpression drives circuit-localized kinase signaling

One of the most recently discovered kinases with a critical role in learning and memory is Meng-Po (MP), a homolog of human SBK1 (Nara et al., 2001; Lee et al., 2018). Meng-Po synergizes with PKA signaling in Kenyon cells, and improves learning and memory when overexpressed in these neurons (Lee et al., 2018). We previously discovered Meng-Po overexpression (MP^{OE}) results in striking PKA signaling induction in the axonal lobes, most prominently in the α′1, β′1, and γ3 connectivity nodes of normally heightened PKA signaling (Sears and Broadie, 2022). Since SBK1 is predicted by gene ontology strategies to enable serine/threonine kinase activity (Gaudet et al., 2011), we hypothesized that ERK signaling might also increase with MP overexpression, including expansion into γ lobe domains, and potentially somata and calyx regions. Consistently, we find MP^{OE} increases ERK signaling in the lobes, somata, and calyx (Fig. 9). In the lobes, new ERK-SPARK puncta appear in the γ1 and γ5 connectivity nodes (Fig. 9*A*), with similar circuit localization to the activity-dependent NaChBac and TRPA1 inductions (Figs. 6*C*, 7*C*). Quantification shows new ERK signaling from MP^{OE} in the γ1 and γ5 connectivity nodes, both with significant (γ1: $p = 0.000311$, Mann–Whitney $U = 0$; γ5: $p = 0.000155$, Mann–Whitney $U = 0$) elevations of ERK-SPARK puncta compared to the driver control (Fig. 9*B*). However, we still find little ERK signaling in the α′1 or β′1 nodes, where PKA signaling is heightened (compare Fig. 1*A*, top to 9*A*, bottom). These results show that overexpression of a PKA-associated kinase improving learning/memory induces localized ERK signaling within Kenyon cells in the underlying circuit.

In the somata, enlarged ERK-SPARK puncta are induced by MP^{OE} within both the Trio− and Trio+ Kenyon cells (Fig. 9*C*). Quantification shows the few ERK-SPARK puncta in the control somata are increased significantly >8-fold by MP^{OE} ($p = 0.00117$, Mann–Whitney $U = 0$; Fig. 9*D*). Dramatic ERK signaling is also induced in the calyx, in Trio− and immediately surrounding regions, with ERK-SPARK puncta concentrated in restricted regions at the periphery (Fig. 9*C*). Quantification shows significant >40-fold elevation in the number of ERK-SPARK puncta with MP^{OE} ($p = 0.000400$; Fig. 9*E*). Given this strong MP-dependent induction of ERK signaling, we wondered if MP might also drive PKA signaling in somata and calyx. MP^{OE} strongly increases PKA signaling in the somata, but the calyx shows no consistent change (Fig. 9*F*). The induced puncta are especially large, suggesting much of the PKA-SPARK biosensor is phosphorylated. Quantification shows significantly more

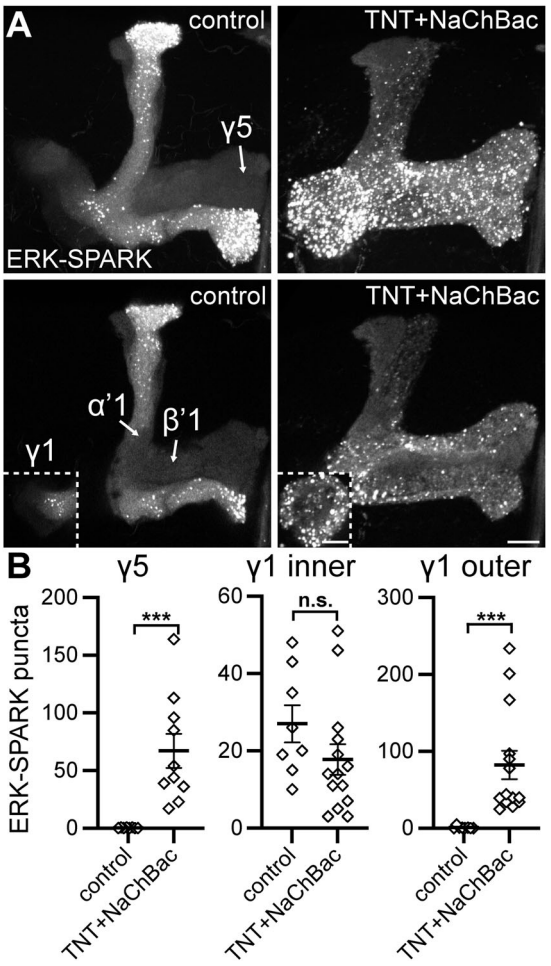

Figure 8. Synaptic output block with potentiated activity rebalances ERK signaling. ***A***, ERK-SPARK imaging in Kenyon cell axon lobes in the OK107-Gal4 driver control (left) and with driven co-expression of both tetanus toxin light chain (TNT) to block Kenyon cell neurotransmission and the voltage-gated Na^+ channel (NaChBac) to also potentiate Kenyon cell activity at the same time (TNT + NaChBac; right). The upper panels show the full z stack projections, whereas the lower panels show single optical slices. The dashed line insets (bottom panels) display adjacent γ1/pedunculus domains. ***B***, Quantification of ERK-SPARK puncta in the indicated circuit domains. Note inner and outer γ1 domain differences. Images display lobes in the rostral portion of the brain and the more caudal γ1/pedunculus. All individual data points shown with mean ± SEM. Significance from Mann–Whitney tests: ***$p < 0.001$ and not statistically significant (n.s.). Scale bars: 10 µm.

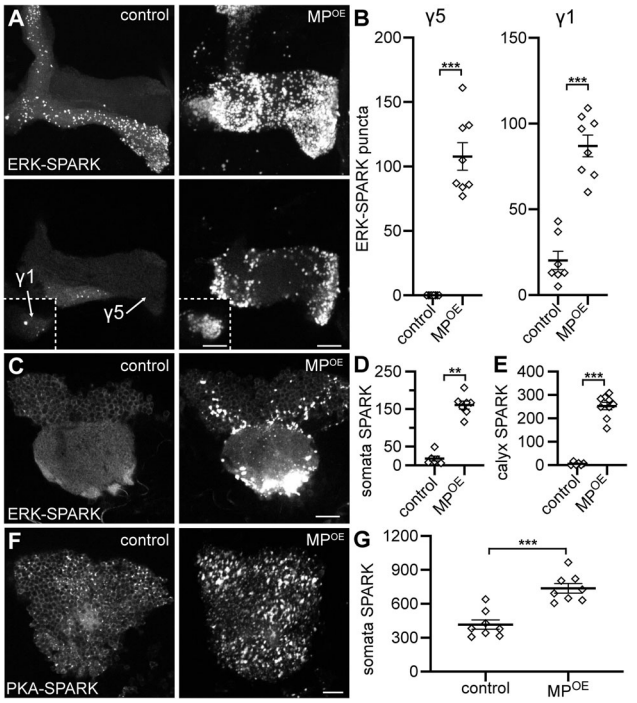

Figure 9. Meng-Po/SBK1 overexpression dramatically elevates kinase signaling. ***A***, ERK-SPARK imaging in Kenyon cell axon lobes in OK107-Gal4 driver control (left) and driving Meng-Po overexpression (MP^{OE}, right). Upper panels are z stack projections, and lower panels are single optical slices. Dashed line insets display the γ1/pedunculus. ***B***, Quantification of ERK-SPARK puncta in indicated nodes. ***C***, ERK-SPARK in Kenyon cell somata and calyx in the same conditions. Quantification of ERK-SPARK puncta in somata (***D***) and calyx (***E***). ***F***, PKA-SPARK imaging in Kenyon cell somata in OK107-Gal4 driver control (left) and driving Meng-Po overexpression (MP^{OE}, right). ***G***, Quantification of PKA-SPARK puncta in Kenyon cell somata. Images are z-projections (top two panels) or single slices. All individual data points shown with mean ± SEM. Significance in Mann–Whitney tests: **$p < 0.01$ and ***$p < 0.001$. Scale bars: 10 µm.

PKA-SPARK puncta with MP^{OE} compared to the driver controls ($p = 0.000622$, Mann–Whitney $U = 2$; Fig. 9*G*). Thus, MP^{OE} induces PKA signaling in the axonal lobes (Sears and Broadie, 2022) as well as Trio− and Trio+ somata. Taken together, these results show that Meng-Po/SBK1 activates both PKA and ERK signaling, but differentially in circuit-localized connectivity nodes. These discrete induction domains are similar between NaChBac/TRPA1 elevated circuit activity and Meng-Po overexpression manipulations, leading us to next test whether hyperexcitable behavioral models display comparably heightened kinase signaling.

A seizure model exhibits heightened circuit-localized PKA/ERK signaling

The above results suggest consistent rules for activity-dependent kinase signaling, so we sought a hyperexcitable disease model to test this relationship. The *Drosophila* "bang-sensitive" epilepsy models (Benzer, 1971; Ganetzky and Wu, 1982; Pavlidis and Tanouye, 1995) show characteristic seizure behaviors and refractory recovery periods (Tan et al., 2004; Reynolds, 2018). The *easily shocked* (*eas*) mutants manifest these behaviors (Ganetzky and Wu, 1982; Pavlidis et al., 1994; Chaturvedi et al., 2022), with recordings showing hyperexcitable neurons activated at lowered stimulation thresholds (Kuebler et al., 2001). Although *eas* mutants show altered mushroom body morphology, this developmental defect is independent of hyperexcitability and seizure phenotypes (Pavlidis et al., 1994; Pascual et al., 2005). With PKA-SPARK, we find dramatically elevated PKA signaling in the *eas* mutants compared to genetic background controls (Fig. 10*A*). In axonal lobes, we find *eas* mutants expand PKA signaling in α/β domains, a small increase in the β'1 node, and γ3 induction (Fig. 10*A*, left). Quantification reveals a significant ($p = 0.0164$; Mann–Whitney $U = 46$) increase in PKA-SPARK puncta in β'1, as well as new induction in both β2 ($p = 0.00188$; Mann–Whitney $U = 8.5$; >40-fold increase) and γ3 ($p = 0.0254$; Mann–Whitney $U = 51$; >25-fold increase) connectivity nodes (Fig. 10*B*). In the postsynaptic calyx, we likewise find increased PKA signaling in the *eas* seizure model, with clustered and enlarged puncta (Fig. 10*A*, right). Quantification shows *eas* mutants have a significant increase in calyx PKA-SPARK puncta ($p = 0.00186$; Mann–Whitney $U = 4$), often with particularly large puncta (Fig. 10*A,B*; right). These highly localized focal phenotypes may indicate enhanced activity-induced local tetanic firing events in the *eas* mutant seizure model.

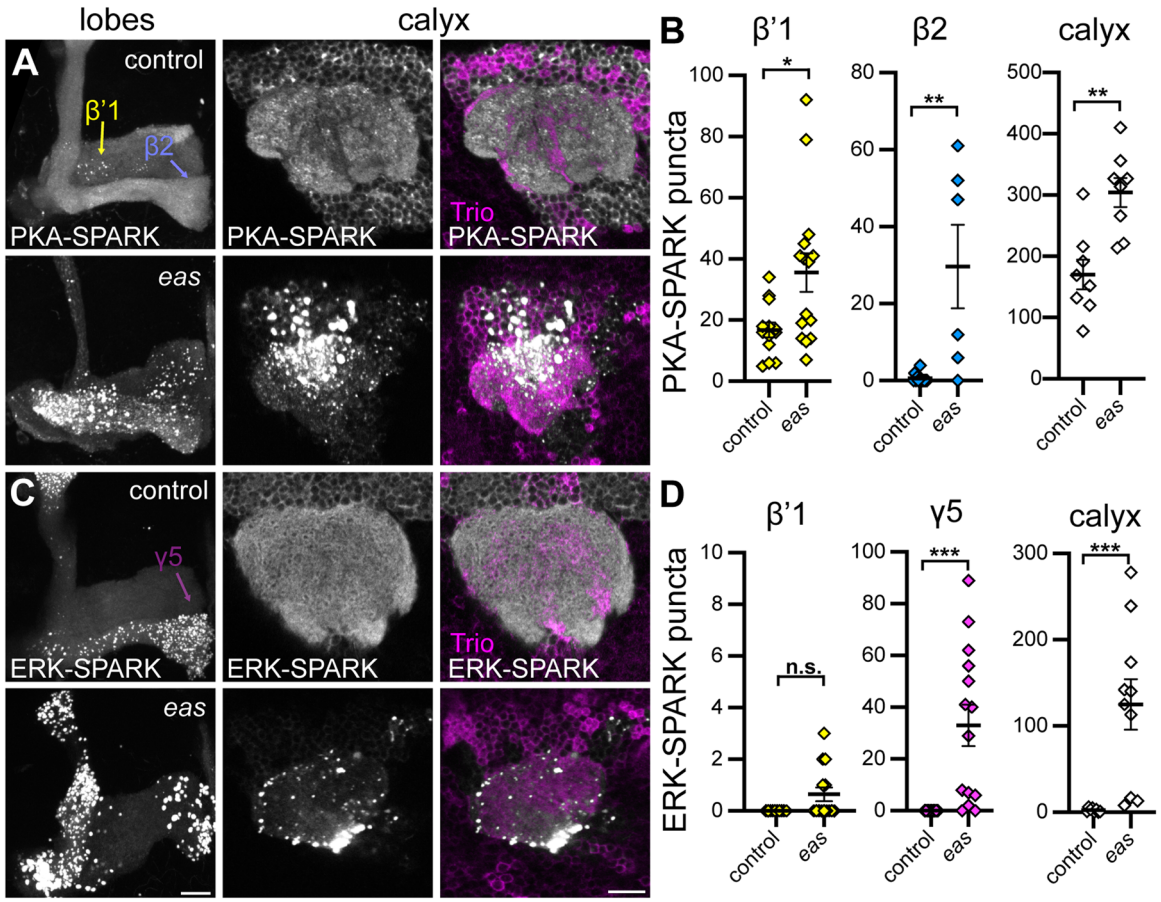

Figure 10. Seizure model exhibits differentially expanded PKA and ERK signaling. ***A***, PKA-SPARK imaging in Kenyon cells in the OK107-Gal4 driver control (top) and in the *eas*^{2} mutant bang-sensitive epileptic seizure model (bottom) within the presynaptic axon lobes (left column), the postsynaptic calyx (middle column), and with anti-Trio (magenta) co-labeling in the merged images (right column). ***B***, Quantification of the number of PKA-SPARK puncta in the indicated circuit domains. ***C***, ERK-SPARK imaging under identical conditions, with Kenyon cell circuit locations separated and co-labeled as above. ***D***, Quantification of the ERK-SPARK puncta in the indicated circuit domains. Images are z-projections (lobes) or single slices (calyx). All individual data points shown with mean ± SEM. Significance from Mann–Whitney tests: *$p < 0.05$, **$p < 0.01$, ***$p < 0.001$, and not statistically significant (n.s.). Scale bars: 10 µm.

With ERK-SPARK, we find differentially heightened ERK signaling in separable circuit-localized connectivity nodes in the *eas* mutants compared to genetic background controls (Fig. 10*C*). We again find selective lobe ERK signaling in the controls, largely restricted to α/β domains (Fig. 10*C*, left). Many nodes show no change in the seizure model, whereas others (e.g., γ5) exhibit dramatic upregulation of ERK-SPARK puncta, reminiscent of above NaChBac and MP^{OE} results. Quantification shows variable changes in the β'1 node, but no significant overall alteration, whereas ERK-SPARK puncta in the γ5 node are significantly ($p = 0.0000642$; Mann–Whitney $U = 10$) elevated in *eas* mutants compared to controls (Fig. 10*D*, left). In the postsynaptic calyx, control animals lack detectable ERK signaling, whereas the seizure model displays clearly induced ERK signaling (Fig. 10*C*, right). We find *eas* mutants have highly elevated ERK signaling in the Trio− α/β regions and in the periphery of the postsynaptic calyx. Quantification shows greatly increased ERK-SPARK puncta in the *eas* mutant calyx, with a significant >50-fold elevation compared to the genetic background controls ($p = 0.0000457$; Mann–Whitney $U = 0$; Fig. 10*D*, right). Taken together, these results reveal heightened Kenyon cell kinase signaling in the *eas* seizure model that is similar to both elevated NaChBac/TRPA activity and MP^{OE} improved learning/memory conditions, suggesting that the elevated activity-dependent PKA and ERK signaling plasticity in circuit-localized connectivity nodes conforms to a consistent topographical modulation.

Discussion

This study reveals a consistent kinase signaling framework that enables plasticity within vastly expandable, but nevertheless limited and coordinated, spatiotemporal limits. Baseline signaling is distinct between PKA and ERK within presynaptic nodes (Fig. 1), which have differential signaling roles (Zars et al., 2000; Buchanan and Davis, 2010). The SPARK biosensors uncover kinase signaling that is not limited to comparisons of pre-stimulus and poststimulus imaging (Gervasi et al., 2010; Tang and Yasuda, 2017; Zhang et al., 2018a,b; Sears and Broadie, 2020). In mice, ERK signaling is similarly heightened in the hippocampus (Ortiz et al., 1995), with differential PKA and ERK baseline signaling in neuronal subpopulations (Sindreu et al., 2007). Since both are downstream effectors of Ca^{2+} and cAMP (Impey et al., 1999; Lee, 2015), the differences in baseline signaling set the stage for circuit responsiveness. PKA regulation of ERK is contextual, with PKA phosphorylation of Raf reducing ERK signaling, as well as PKA targets positively regulating ERK (Mischak et al., 1996; Sprenkle et al., 1997; Dhillon et al., 2002; Jain et al., 2018). Thus, preexisting, baseline PKA signaling may suppress circuit-localized ERK function,

while ERK may be permissive for PKA signaling (compare Figs. 1, 6, 7). Baseline excitability may also contribute, as α'/β' lobes are more excitable than other lobes (Turner et al., 2008; Inada et al., 2017; Leinwand and Scott, 2021). Our results suggest a maintained spatial organization of kinase signaling within circuitry that is poised for coordinated responses to multimodal sensory input and the induction of appropriate behavioral outputs. We suggest that baseline signaling interacts to enable higher order processing, reflected in topographical arrays mapped to specific connectivity nodes poised to respond with experience-dependent changes.

As circuit-targeted ERK activation strategies, we increased pathway signaling at two levels; Raf gain-of-function (Raf^{gof}), upstream in the MAPK regulatory pathway, and constitutively-active ERK (Fig. 3; Brand and Perrimon, 1994; Brunner et al., 1994; Sun et al., 2020). Both increase ERK signaling, but not to the degree we expected from analogous PKA experiments (Kiger et al., 1999; Sears et al., 2019). The activated ERK (Rl^{Sem}) may more weakly elevate signaling (Brunner et al., 1994), which may account for some differences with Raf^{gof}. The Raf^{gof} transgene also lacks terminal regulatory regions (Heidecker et al., 1992; Brand and Perrimon, 1994), which could result in stronger activation. However, negative feedback differences at sequential pathway tiers may also be critical (Klomp et al., 2021), with regulation downstream of Raf^{gof} expected due to convergent signaling. Alternatively, Rl^{Sem} may be comparatively lower in expression. Intriguingly, in the Raf^{gof} condition somata ERK signaling is induced to much greater degree with low PKA signaling (compare Figs. 1, 3), suggesting interactive signaling regulation between the two pathways. Since Raf^{gof} drives ERK signaling in lower baseline PKA signaling circuit domains, we suggest that baseline heightened PKA signaling restricts ERK induction. While some PKA inhibitory residues are expected to be missing with Raf^{gof} (notably Ser-259/Ser-346; Dhillon et al., 2002), Ser-621/Ser-701 persist as sites of potential PKA phosphorylation and pathway cross-talk inhibition (Mischak et al., 1996; Sprenkle et al., 1997). Comparing Raf^{gof} and Rl^{Sem} manipulations in the context of additional kinase pathways may expand upon baseline contributions to circuit-localized signaling and its control over ERK induction.

Targeted tetanus toxin (TNT) and $shibire^{ts}$ blockade of Kenyon cell synaptic transmission dramatically increases ERK signaling in restricted connectivity nodes (Fig. 5). Preventing output allows for the analysis of feedback control over kinase signaling, and possibly lateral Kenyon cross talk, with parallels to expanded cAMP-PKA signaling (Hackley et al., 2018; Manoim et al., 2022; Sears and Broadie, 2022). Our results suggest circuit-localized suppression of ERK signaling via feedback/lateral control mechanisms. This localized synaptic transmission-dependent ERK signaling may be determined by local baseline signaling levels, since the same neurons with heightened baseline ERK signaling still display enhanced signaling (compare Figs. 1, 5). Interestingly, this compartment is in the most proximal circuit output domain, thought to act as a "toggle switch" regulating behavioral responses by inhibiting more distal output regions (Perisse et al., 2016; Modi et al., 2020). Our results suggest that activity-dependent lateral signaling control via compartment-selective kinase signaling, built upon baseline signaling, may determine local plasticity of essential gatekeeping circuitry. This circuit-localized function appears similar to local interneurons argued to act as gatekeepers of hippocampal excitation (He et al., 2022; Poll and Fuhrmann, 2022), suggesting a conserved strategy for higher order association. Further inquiries into output-dependent, selective kinase signaling will provide more insights into circuit-localized plasticity.

Kinase signaling in select regions can be enormously increased by potentiating circuit electrical activity, showing the capacity for activity-induced signaling (Fig. 6). NaChBac induction potentiates normal circuit activity, and can even improve performance (Lin et al., 2021). Thermogenetic TRPA1 manipulations reveal similar activity-dependent processes (Pulver et al., 2009). Importantly, heightened activity causes a more comprehensive, yet still circuit-localized, signaling induction compared to direct kinase pathway activation (compare Figs. 3, 6, 7), showing the orchestration of circuit activity-dependent signaling. Combining TNT and NaChBac suggests cell-autonomous, or at least feedback-independent, activity regulated localized signaling (Fig. 8), although interpretation is limited by morphological defects with this manipulation. Circuit-level regulation is likely determined via local neuromodulatory and GABAergic inhibitory inputs, which are known to function as experience-dependent regulators of local circuit activity and kinase signaling, in addition to compartment-specific plasticity (Liu et al., 2007; Tanaka et al., 2008; Liu and Davis, 2009; Lee et al., 2011; Aso et al., 2014b; Modi et al., 2020). For example, mushroom body lobe compartmentalized plasticity and cAMP-dependent regulation downstream of dopamine circuit activation have been described (Boto et al., 2014; Hige et al., 2015; Louis et al., 2018; Handler et al., 2019). Moreover, brain states of arousal, awareness, stress, and nutrition may contribute to kinase signaling induction, while combinatorial and multimodal experience may contribute to interactive pathways (Androschuk et al., 2018; Okray et al., 2023; Titos et al., 2023). Our work here provides a foundation to investigate how the wider integrated brain circuitry, experience history, and behavioral states work to determine activity-dependent higher order circuit signaling. Future studies will test cell autonomous and local circuit contributions to connectivity node Kenyon cell signaling.

The targeted overexpression of Meng-Po kinase (human SBK1) dramatically increases circuit-localized ERK and PKA signaling (Fig. 9). This same Meng-Po^{OE} condition improves learning and memory performance (Lee et al., 2018). Thus, Kenyon cells have an untapped capacity for kinase signaling, and the highly plastic *Drosophila* learning/memory circuit is an excellent model to test for pharmacological activation and ancillary learning gene contributions. Importantly, SBK1 is enriched in the mammalian hippocampus (Nara et al., 2001), suggesting conserved kinase function in learning and memory. SBK1 function is predicted to facilitate serine/threonine kinase activity (Gaudet et al., 2011), and SBK1 promotes ERK signaling in a cancer model (Chen et al., 2023). Taken together, these investigations suggest conserved SBK1-dependent learning and memory, and an untapped learning and memory kinase potential dependent on SBK1. In the context of our kinase functional imaging (Fig. 9), we may be witnessing an improved utilization of activity-dependent learning and memory circuitry through induction of circuit-localized kinase signaling. Consistently, cell-targeted NaChBac and Meng-Po^{OE} also augment *Drosophila* learning (Lee et al., 2018; Lin et al., 2021). We suggest Meng-Po/SBK1 acts as an ancillary kinase that sets the signaling threshold for PKA and ERK serine/threonine kinases. We predict targeted upregulation of Meng-Po/SBK1 could be a therapeutic strategy to support kinase signaling when and where it normally occurs.

An epileptic seizure model increases circuit-localized kinase signaling (Fig. 10). Heightened excitability may occur more

readily in connectivity nodes where sensory input modalities converge on behavioral outputs (Davis, 2004; Gerber et al., 2004; Tanaka et al., 2008; Aso et al., 2014a,b). While we cannot rule out the contribution of Kenyon cell morphological defects in these *eas* mutants, such background defects are proven unrelated to seizure behavior (Pascual et al., 2005). Epilepsy patients exhibit low-threshold experience-dependent triggers (Novakova et al., 2013; Hanif and Musick, 2021; Katyayan and Diaz-Medina, 2021), and subconvulsive kindling stimulation in rodents promotes seizures (Goddard, 1967; Goddard et al., 1969; Leech and McIntyre, 1976). Kindling occurs more readily in rodent seizure models (Green and Seyfried, 1991), and *Drosophila* models similarly experience seizures at lower thresholds (Kuebler et al., 2001). Interestingly, some rodent seizure models in seizure-free conditions show significantly quicker decision-making and improved learning (Holmes et al., 1990; Gutekunst et al., 1993). This may suggest improved utilization of learning and memory circuitry in the absence of seizures, consistent with NaChBac and Meng-Po^{OE} manipulations (compare Figs. 6, 7, 9, 10; Lee et al., 2018; Lin et al., 2021). In temporal lobe epilepsy, hippocampal seizure foci are common (Spencer et al., 1984; Bauman et al., 2019) and have been shown to acutely promote hippocampal signaling (Baraban et al., 1993; Blüthgen et al., 2017), but a sufficient interval without seizures blunts signaling (Houser et al., 2008). We may therefore expect reduced KC signaling in some regions after seizure induction. Alternatively, increased signaling could indicate maladaptation and hyperexcitability. Future investigations of additional seizure models and kinase-kinase interactions will reveal experience-dependent mechanisms controlling local circuit connectivity signaling nodes before, during, and after behavior adaptations.

References

Androschuk A, He RX, Weber S, Rosenfelt C, Bolduc FV (2018) Stress odorant sensory response dysfunction in Drosophila Fragile X syndrome mutants. Front Mol Neurosci 11:242.

Aso Y, et al. (2014a) Mushroom body output neurons encode valence and guide memory-based action selection in Drosophila. Elife 3:e04580.

Aso Y, et al. (2014b) The neuronal architecture of the mushroom body provides a logic for associative learning. Elife 3:e04577.

Baraban JM, Fiore RS, Sanghera JS, Paddon HB, Pelech SL (1993) Identification of p42 mitogen-activated protein kinase as a tyrosine kinase substrate activated by maximal electroconvulsive shock in hippocampus. J Neurochem 60:330–336.

Bauman K, Devinsky O, Liu AA (2019) Temporal lobe surgery and memory: lessons, risks, and opportunities. Epilepsy Behav 101:106596.

Benzer S (1971) From the gene to behavior. J Am Med Assoc 218:1015–1022.

Biggs WH, Zavitz KH, Dickson B, van der Straten A, Brunner D, Hafen E, Zipursky SL (1994) The Drosophila rolled locus encodes a MAP kinase required in the sevenless signal transduction pathway. EMBO J 13: 1628–1635.

Blitzer RD, Connor JH, Brown GP, Wong T, Shenolikar S, Iyengar R, Landau EM (1998) Gating of CaMKII by cAMP-regulated protein phosphatase activity during LTP. Science 280:1940–1942.

Blüthgen N, van Bentum M, Merz B, Kuhl D, Hermey G (2017) Profiling the MAPK/ERK dependent and independent activity regulated transcriptional programs in the murine hippocampus in vivo. Sci Rep 7:45101.

Boto T, Louis T, Jindachomthong K, Jalink K, Tomchik SM (2014) Dopaminergic modulation of cAMP drives nonlinear plasticity across the Drosophila mushroom body lobes. Curr Biol 24:822–831.

Brand AH, Perrimon N (1994) Raf acts downstream of the EGF receptor to determine dorsoventral polarity during Drosophila oogenesis. Genes Dev 8:629–639.

Brunner D, Oellers N, Szabad J, Biggs WH, Zipursky SL, Hafen E (1994) A gain-of-function mutation in Drosophila MAP kinase activates multiple receptor tyrosine kinase signaling pathways. Cell 76:875–888.

Buchanan ME, Davis RL (2010) A distinct set of Drosophila brain neurons required for neurofibromatosis type 1-dependent learning and memory. J Neurosci 30:10135–10143.

Chaturvedi R, Stork T, Yuan C, Freeman MR, Emery P (2022) Astrocytic GABA transporter controls sleep by modulating GABAergic signaling in Drosophila circadian neurons. Curr Biol 32:1895–1908.e5.

Chen X, Sun Z, Zhou S, Jiang W, Li J, Song G, Zhu X (2023) SH3 domain-binding kinase 1 promotes proliferation and inhibits apoptosis of cervical cancer via activating the Wnt/β-catenin and Raf/ERK1/2 signaling pathways. Mol Carcinog. 62:1147–1162.

Cole AJ (2000) Is epilepsy a progressive disease? The neurobiological consequences of epilepsy. Epilepsia 41:S13–22.

Connolly JB, Roberts IJ, Armstrong JD, Kaiser K, Forte M, Tully T, O'Kane CJ (1996) Associative learning disrupted by impaired Gs signaling in Drosophila mushroom bodies. Science 274:2104–2107.

Crittenden JR, Skoulakis EMC, Han KA, Kalderon D, Davis RL (1998) Tripartite mushroom body architecture revealed by antigenic markers. Learn Mem 5:38–51.

Davis RL (2004) Olfactory learning. Neuron 44:31–48.

Davis RL (2023) Learning and memory using Drosophila melanogaster: a focus on advances made in the fifth decade of research. Genetics 224:1–22.

Dear ML, Shilts J, Broadie K (2017) Neuronal activity drives FMRP- and HSPG-dependent matrix metalloproteinase function required for rapid synaptogenesis. Sci Signal 10:eaan3181.

Dhillon AS, Meikle S, Yazici Z, Eulitz M, Kolch W (2002) Regulation of Raf-1 activation and signalling by dephosphorylation. EMBO J 21:64–71.

Doll CA, Vita DJ, Broadie K (2017) Fragile X mental retardation protein requirements in activity-dependent critical period neural circuit refinement. Curr Biol 27:2318–2330.

Ganetzky B, Wu C-F (1982) Indirect suppression involving behavioral mutants with altered nerve excitability in Drosophila melanogaster. Genetics 100:597–614.

Gaudet P, Livstone MS, Lewis SE, Thomas PD (2011) Phylogenetic-based propagation of functional annotations within the gene ontology consortium. Brief Bioinform 12:449–462.

Gerber B, Tanimoto H, Heisenberg M (2004) An engram found? Evaluating the evidence from fruit flies. Curr Opin Neurobiol 14:737–744.

Gervasi N, Tchénio P, Preat T (2010) PKA dynamics in a Drosophila learning center: coincidence detection by rutabaga adenylyl cyclase and spatial regulation by dunce phosphodiesterase. Neuron 65:516–529.

Giese KP, Mizuno K (2013) The roles of protein kinases in learning and memory. Learn Mem 20:540–552.

Goddard GV (1967) Development of epileptic seizures through brain stimulation at low intensity. Nature 214:1020–1021.

Goddard GV, McIntyre DC, Leech CK (1969) A permanent change in brain function resulting from daily electrical stimulation. Exp Neurol 25:295–330.

Green RC, Seyfried TN (1991) Kindling susceptibility and genetic seizure predisposition in inbred mice. Epilepsia 32:22–26.

Gutekunst CA, Hartney A, Rees HD, Green RC (1993) Lack of strain differences in spatial learning among seizure-prone and seizure-resistant mice. Behav Genet 23:385–389.

Haag J, Arenz A, Serbe E, Gabbiani F, Borst A (2016) Complementary mechanisms create direction selectivity in the fly. Elife 5:e17421.

Hackley CR, Mazzoni EO, Blau J (2018) cAMPr: a single-wavelength fluorescent sensor for cyclic AMP. Sci Signal 11:eaah3738.

Hamada FN, Rosenzweig M, Kang K, Pulver SR, Ghezzi A, Jegla TJ, Garrity PA (2008) An internal thermal sensor controlling temperature preference in Drosophila. Nature 454:217–220.

Handler A, Graham TGW, Cohn R, Morantte I, Siliciano AF, Zeng J, Li Y, Ruta V (2019) Distinct dopamine receptor pathways underlie the temporal sensitivity of associative learning. Cell 178:60–75.e19.

Hanif S, Musick ST (2021) Reflex epilepsy. Aging Dis 12:1010–1020.

He L, Caudill MS, Jing J, Wang W, Sun Y, Tang J, Jiang X, Zoghbi HY (2022) A weakened recurrent circuit in the hippocampus of Rett syndrome mice disrupts long-term memory representations. Neuron 110:1689–1699.e6.

Heidecker G, Kölch W, Morrison DK, Rapp UR (1992) The role of Raf-1 phosphorylation in signal transduction. Adv Cancer Res 58:53–73.

Hige T, Aso Y, Modi MN, Rubin GM, Turner GC (2015) Heterosynaptic plasticity underlies aversive olfactory learning in Drosophila. Neuron 88:985–998.

Holmes GL, Thompson JL, Marchi TA, Gabriel PS, Hogan MA, Carl FG, Feldman DS (1990) Effects of seizures on learning, memory, and behavior in the genetically epilepsy-prone rat. Ann Neurol 27:24–32.

Houser CR, Huang CS, Peng Z (2008) Dynamic seizure-related changes in extracellular signal-regulated kinase activation in a mouse model of temporal lobe epilepsy. Neuroscience 156:222–237.
Impey S, Obrietan K, Storm DR (1999) Making new connections: role of ERK/MAP kinase signaling in neuronal plasticity. Neuron 23:11–14.
Inada K, Tsuchimoto Y, Kazama H (2017) Origins of cell-type-specific olfactory processing in the Drosophila mushroom body circuit. Neuron 95: 357–367.e4.
Jain R, Watson U, Vasudevan L, Saini DK (2018) ERK activation pathways downstream of GPCRs. Int Rev Cell Mol Biol 338:79–109.
Jeong J, Lee J, Kim J-H, Lim C (2021) Metabolic flux from the Krebs cycle to glutamate transmission tunes a neural brake on seizure onset. PLoS Genet 17:e1009871.
Katyayan A, Diaz-Medina G (2021) Epilepsy: epileptic syndromes and treatment. Neurol Clin 39:779–795.
Khan R, Kulasiri D, Samarasinghe S (2021) Functional repertoire of protein kinases and phosphatases in synaptic plasticity and associated neurological disorders. Neural Regen Res 16:1150–1157.
Kiger JA, Eklund JL, Younger SH, O'Kane CJ (1999) Transgenic inhibitors identify two roles for protein kinase a in Drosophila development. Genetics 152:281–290.
Kitamoto T (2001) Conditional modification of behavior in Drosophila by targeted expression of a temperature-sensitive shibire allele in defined neurons. J Neurobiol 47:81–92.
Klomp JE, Klomp JA, Der CJ (2021) The ERK mitogen-activated protein kinase signaling network: the final frontier in RAS signal transduction. Biochem Soc Trans 49:253–267.
Koenig JH, Saito K, Ikeda K (1983) Reversible control of synaptic transmission in a single gene mutant of Drosophila melanogaster. J Cell Biol 96: 1517–1522.
Kuebler D, Zhang H, Ren X, Tanouye MA (2001) Genetic suppression of seizure susceptibility in Drosophila. J Neurophysiol 86:1211–1225.
Lai YW, Miyares RL, Liu LY, Chu SY, Lee T, Yu HH (2022) Hormone-controlled changes in the differentiation state of post-mitotic neurons. Curr Biol 32:2341–2348.e3.
Lee D (2015) Global and local missions of cAMP signaling in neural plasticity, learning, and memory. Front Pharmacol 6:161.
Lee P-T, Lin H-W, Chang Y-H, Fu T-F, Dubnau J, Hirsh J, Lee T, Chiang A-S (2011) Serotonin-mushroom body circuit modulating the formation of anesthesia-resistant memory in Drosophila. Proc Natl Acad Sci U S A 108:13794–13799.
Lee P-T, Lin G, Lin W-W, Diao F, White BH, Bellen HJ (2018) A kinase-dependent feedforward loop affects CREBB stability and long term memory formation. Elife 7:e33007.
Leech CK, McIntyre DC (1976) Kindling rates in inbred mice: an analog to learning? Behav Biol 16:439–452.
Leinwand SG, Scott K (2021) Juvenile hormone drives the maturation of spontaneous mushroom body neural activity and learned behavior. Neuron 109:1836–1847.e5.
Li F, et al. (2020) The connectome of the adult Drosophila mushroom body provides insights into function. Elife 9:e62576.
Li Y, et al. (2022) Metabolic control of progenitor cell propagation during Drosophila tracheal remodeling. Nat Commun 13:2817.
Li W, Tully T, Kalderon D (1996) Effects of a conditional Drosophila PKA mutant on olfactory learning and memory. Learn Mem 2:320–333.
Lin H-W, Chen C-C, de Belle JS, Tully T, Chiang A-S (2021) CREBA and CREBB in two identified neurons gate long-term memory formation in Drosophila. Proc Natl Acad Sci U S A 118:e2100624118.
Link E, Edelmann L, Chou JH, Binz T, Yamasaki S, Eisel U, Baumert M, Südhof TC, Niemann H, Jahn R (1992) Tetanus toxin action: inhibition of neurotransmitter release linked to synaptobrevin proteolysis. Biochem Biophys Res Commun 189:1017–1023.
Liu L-Y, Long X, Yang C-P, Miyares RL, Sugino K, Singer RH, Lee T (2019) Mamo decodes hierarchical temporal gradients into terminal neuronal fate. Elife 8:e48056.
Liu X, Davis RL (2009) The GABAergic anterior paired lateral neuron suppresses and is suppressed by olfactory learning. Nat Neurosci 12:53–59.
Liu X, Krause WC, Davis RL (2007) GABAA receptor RDL inhibits Drosophila olfactory associative learning. Neuron 56:1090–1102.
Louis T, Stahl A, Boto T, Tomchik SM (2018) Cyclic AMP-dependent plasticity underlies rapid changes in odor coding associated with reward learning. Proc Natl Acad Sci U S A 115:E448–E457.
Mabuchi Y, Cui X, Xie L, Kim H, Jiang T, Yapici N (2023) Visual feedback neurons fine-tune Drosophila male courtship via GABA-mediated inhibition. Curr Biol 33:3896–3910.e7.
Manoim JE, Davidson AM, Weiss S, Hige T, Parnas M (2022) Lateral axonal modulation is required for stimulus-specific olfactory conditioning in Drosophila. Curr Biol 32:4438–4450.e5.
Mao L-M, Wang JQ (2016) Synaptically localized mitogen-activated protein kinases: local substrates and regulation. Mol Neurobiol 53:6309–6315.
Mischak H, Seitz T, Janosch P, Eulitz M, Steen H, Schellerer M, Philipp A, Kolch W (1996) Negative regulation of Raf-1 by phosphorylation of serine 621. Mol Cell Biol 16:5409–5418.
Modi MN, Shuai Y, Turner GC (2020) The Drosophila mushroom body: from architecture to algorithm in a learning circuit. Annu Rev Neurosci 43: 465–484.
Nara K, Akasako Y, Matsuda Y, Fukazawa Y, Iwashita S, Kataoka M, Nagai Y (2001) Cloning and characterization of a novel serine/threonine protein kinase gene expressed predominantly in developing brain. Eur J Biochem 268:2642–2651.
Nitabach MN, Wu Y, Sheeba V, Lemon WC, Strumbos J, Zelensky PK, White BH, Holmes TC (2006) Electrical hyperexcitation of lateral ventral pacemaker neurons desynchronizes downstream circadian oscillators in the fly circadian circuit and induces multiple behavioral periods. J Neurosci 26: 479–489.
Novakova B, Harris PR, Ponnusamy A, Reuber M (2013) The role of stress as a trigger for epileptic seizures: a narrative review of evidence from human and animal studies. Epilepsia 54:1866–1876.
Okray Z, Jacob PF, Stern C, Desmond K, Otto N, Talbot CB, Vargas-Gutierrez P, Waddell S (2023) Multisensory learning binds neurons into a cross-modal memory engram. Nature 617:777–784.
Ortiz J, Harris HW, Guitart X, Terwilliger RZ, Haycock JW, Nestler EJ (1995) Extracellular signal-regulated protein kinases (ERKs) and ERK kinase (MEK) in brain: regional distribution and regulation by chronic morphine. J Neurosci 15:1285–1297.
Pardo-Garcia TR, Gu K, Woerner RKR, Dus M (2023) Food memory circuits regulate eating and energy balance. Curr Biol 33:215–227.e3.
Pascual A, Chaminade M, Préat T (2005) Ethanolamine kinase controls neuroblast divisions in Drosophila mushroom bodies. Dev Biol 280:177–186.
Pavlidis P, Tanouye MA (1995) Seizures and failures in the giant fiber pathway of Drosophila bang-sensitive paralytic mutants. J Neurosci 15: 5810–5819.
Pavlidis P, Ramaswami M, Tanouye MA (1994) The Drosophila easily shocked gene: a mutation in a phospholipid synthetic pathway causes seizure, neuronal failure, and paralysis. Cell 79:23–33.
Perisse E, Owald D, Barnstedt O, Talbot CB, Huetteroth W, Waddell S (2016) Aversive learning and appetitive motivation toggle feed-forward inhibition in the Drosophila mushroom body. Neuron 90:1086–1099.
Poll S, Fuhrmann M (2022) O-LM interneurons: gatekeepers of pyramidal neuron activity in the hippocampus. Neuron 110:1606–1608.
Pulver SR, Pashkovski SL, Hornstein NJ, Garrity PA, Griffith LC (2009) Temporal dynamics of neuronal activation by channelrhodopsin-2 and TRPA1 determine behavioral output in Drosophila larvae. J Neurophysiol 101:3075–3088.
Reynolds ER (2018) Shortened lifespan and other age-related defects in bang sensitive mutants of Drosophila melanogaster. G3 8:3953–3960.
Rohrbough J, Broadie K (2002) Electrophysiological analysis of synaptic transmission in central neurons of Drosophila larvae. J Neurophysiol 88:847–860.
Schiavo G, Benfenati F, Poulain B, Rossetto O, Polverino de Laureto P, DasGupta BR, Montecucco C (1992) Tetanus and botulinum-B neurotoxins block neurotransmitter release by proteolytic cleavage of synaptobrevin. Nature 359:832–835.
Sears JC, Broadie K (2020) FMRP-PKA activity negative feedback regulates RNA binding-dependent fibrillation in brain learning and memory circuitry. Cell Rep 33:108266.
Sears JC, Broadie K (2022) Temporally and spatially localized PKA activity within learning and memory circuitry regulated by network feedback. eNeuro 9:1–15.
Sears JC, Choi WJ, Broadie K (2019) Fragile X mental retardation protein positively regulates PKA anchor rugose and PKA activity to control actin assembly in learning/memory circuitry. Neurobiol Dis 127:53–64.
Shaheen A, Richter Gorey CL, Sghaier A, Dason JS (2023) Cholesterol is required for activity-dependent synaptic growth. J Cell Sci. 136:jcs261563.

Sindreu CB, Scheiner ZS, Storm DR (2007) Ca2+ -stimulated adenylyl cyclases regulate ERK-dependent activation of MSK1 during fear conditioning. Neuron 53:79–89.
Spencer DD, Spencer SS, Mattson RH, Williamson PD, Novelly RA (1984) Access to the posterior medial temporal lobe structures in the surgical treatment of temporal lobe epilepsy. Neurosurgery 15:667–671.
Sprenkle AB, Davies SP, Carling D, Hardie DG, Sturgill TW (1997) Identification of Raf-1 Ser621 kinase activity from NIH 3T3 cells as AMP-activated protein kinase. FEBS Lett 403:254–258.
Sun L, et al. (2020) Attenuation of epigenetic regulator SMARCA4 and ERK-ETS signaling suppresses aging-related dopaminergic degeneration. Aging Cell 19:e13210.
Sweeney ST, Broadie K, Keane J, Niemann H, O'Kane CJ (1995) Targeted expression of tetanus toxin light chain in Drosophila specifically eliminates synaptic transmission and causes behavioral defects. Neuron 14:341–351.
Tan JS, Lin F, Tanouye MA (2004) Potassium bromide, an anticonvulsant, is effective at alleviating seizures in the Drosophila bang-sensitive mutant bang senseless. Brain Res 1020:45–52.
Tanaka NK, Tanimoto H, Ito K (2008) Neuronal assemblies of the Drosophila mushroom body. J Comp Neurol 508:711–755.
Tang S, Yasuda R (2017) Imaging ERK and PKA activation in single dendritic spines during structural plasticity. Neuron 93:1315–1324.e3.
Taylor SS, Zhang P, Steichen JM, Keshwani MM, Kornev AP (2013) PKA: lessons learned after twenty years. Biochim Biophys Acta 1834:1271–1278.
Titos I, Juginović A, Vaccaro A, Nambara K, Gorelik P, Mazor O, Rogulja D (2023) A gut-secreted peptide suppresses arousability from sleep. Cell 186:1382–1397.e21.
Turner GC, Bazhenov M, Laurent G (2008) Olfactory representations by Drosophila mushroom body neurons. J Neurophysiol 99:734–746.
Turrel O, Rabah Y, Plaçais P-Y, Goguel V, Preat T (2020) Drosophila middle-term memory: amnesiac is required for PKA activation in the mushroom bodies, a function modulated by neprilysin 1. J Neurosci 40:4219–4229.
Vijayakrishnan N, Phillips SE, Broadie K (2010) Drosophila rolling blackout displays lipase domain-dependent and -independent endocytic functions downstream of dynamin. Traffic 11:1567–1578.
von Kriegsheim A, et al. (2009) Cell fate decisions are specified by the dynamic ERK interactome. Nat Cell Biol 11:1458–1464.
Wang Y, Chen Z (2019) An update for epilepsy research and antiepileptic drug development: toward precise circuit therapy. Pharmacol Ther 201:77–93.
Wei T, Ji X, Gao Y, Zhu X, Xiao G (2021) Znt7 RNAi favors RafGOFscrib-/–induced tumor growth and invasion in Drosophila through JNK signaling pathway. Oncogene 40:2217–2229.
Wiegert JS, Bading H (2011) Activity-dependent calcium signaling and ERK-MAP kinases in neurons: a link to structural plasticity of the nucleus and gene transcription regulation. Cell Calcium 49:296–305.
Yamasaki S, Hu Y, Binz T, Kalkuhl A, Kurazono H, Tamura T, Jahn R, Kandel E, Niemann H (1994) Synaptobrevin/vesicle-associated membrane protein (VAMP) of Aplysia californica: structure and proteolysis by tetanus toxin and botulinal neurotoxins type D and F. Proc Natl Acad Sci U S A 91:4688–4692.
Zars T, Fischer M, Schulz R, Heisenberg M (2000) Localization of a short-term memory in Drosophila. Science 288:672–675.
Zhang Q, et al. (2018a) Visualizing dynamics of cell signaling in vivo with a phase separation-based kinase reporter. Mol Cell 69:334–346.e4.
Zhang X, Li Q, Wang L, Liu Z-J, Zhong Y (2018b) Active protection: learning-activated Raf/MAPK activity protects labile memory from Rac1-independent forgetting. Neuron 98:142–155.e4.
Zhao J, Zhang X, Zhao B, Hu W, Diao T, Wang L, Zhong Y, Li Q (2023) Genetic dissection of mutual interference between two consecutive learning tasks in Drosophila. Elife 12:e83516.
Zimmerman JE, Chan MT, Lenz OT, Keenan BT, Maislin G, Pack AI (2017) Glutamate is a wake-active neurotransmitter in Drosophila melanogaster. Sleep 40:zsw046.